



Development of activated carbons derived from wastes: coffee grounds and olive stones as potential porous materials for air depollution

Natalia Czerwinska^{a,*}, Chiara Giosuè^{a,*}, Ines Matos^b, Simona Sabbatini^a, Maria Letizia Ruello^a, Maria Bernardo^b

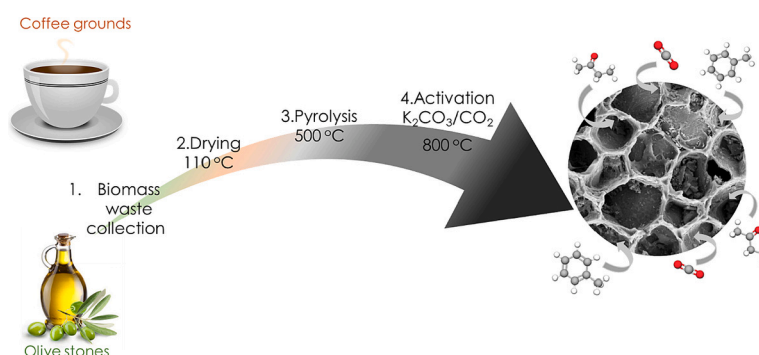
^a Department of Science and Engineering of Matter, Environment and Urban Planning (SIMAU), Università Politecnica delle Marche, Udr INSTM Ancona, Italy

^b LAQV/REQUIMTE, NOVA School of Science and Technology, NOVA University of Lisbon, 2829-516 Caparica, Portugal

HIGHLIGHTS

- A sustainable approach to producing activated carbon from wastes was studied.
- Waste-derived activated carbon can play an important role in air depollution.
- The adsorption potential is correlated with morphological properties.
- Excellent VOCs adsorption capacities up to 3210 mg/g are demonstrated.
- The highest adsorption capacity recorded of CO₂ is 253 mg/g.

GRAPHICAL ABSTRACT



ARTICLE INFO

Editor: Frederic Coulon

Keywords:

Biomass waste
Porous carbons
Adsorption
Indoor air treatment
Pollutants
VOCs

ABSTRACT

Agro-industrial byproducts and food waste necessitate an environmentally friendly way of reducing issues related to their disposal; it is also necessary to recover as much new raw material from these resources as possible, especially when we consider their potential usage as a precursor for preparing depolluting materials, such as activated carbon. In this work, coffee grounds and olive stones were chosen as precursors and the adsorption capacity of the obtained porous carbons for volatile organic compounds (VOCs) was studied. Microporous activated carbons (ACs) were prepared using chemical (K₂CO₃) and physical (CO₂) activation. The influence of the activation process, type, and time of activation was also investigated. Measurements of VOCs adsorption were performed, and methyl-ethyl-ketone (MEK) and toluene were chosen as the model pollutants. The surface areas and total pore volumes of 1487 m²/g and 0.53 cm³/g and 870 m²/g and 0.22 cm³/g for coffee ground carbons and olive stone carbons, respectively, were obtained via chemical activation, whereas physical activation yielded values of 716 m²/g and 0.184 cm³/g and 778 cm² g⁻¹ and 0.205 cm³/g, respectively. As expected, carbons without activation (biochars) showed the smallest surface area, equal to 331 m²/g and 251 m²/g, and, hence, the lowest adsorption capacity. The highest adsorption capacity of MEK (3210 mg/g) and toluene (2618 mg/g) was recorded for chemically activated coffee grounds. Additionally, from the CO₂ isotherms recorded at a low pressure (0.03 bar) and 0 °C, the maximum CO₂ adsorption capacity was equal to 253 mg/g.

* Corresponding authors.

E-mail addresses: n.czerwinska@pm.univpm.it (N. Czerwinska), c.giosue@staff.univpm.it (C. Giosuè).

<https://doi.org/10.1016/j.scitotenv.2024.169898>

Received 26 October 2023; Received in revised form 20 December 2023; Accepted 2 January 2024

Available online 5 January 2024

0048-9697/© 2024 Published by Elsevier B.V.

1. Introduction

Despite modern industry being less polluting than older ones, a serious environmental problem at the local and global scales is represented by fast-growing worldwide development (Ramírez Hernández et al., 2020; Silva et al., 2020a). Furthermore, intensive agriculture produces a relevant environmental impact and must be considered specifically as a polluting productive sector. Countries where industry plays a significant role struggle with the problem of high pollution levels, but emissions from combustion for energy production and transportation are also responsible for increasing levels of harmful pollutants. As reported previously, the indoor air levels of many pollutants may be 2–10 times higher than outdoor levels (Madureira et al., 2009; Žuškin et al., 2009), and people spend approximately 90 % of their time indoors (Nieto-Márquez et al., 2023; Klepeis et al., 2001). In particular, during the pandemic, most workers started engaging in hybrid working schedules, combining working in their usual workplace and from home (Eurostat, 2022). For this reason, it is highly important to reduce harmful components that can have an impact on the environment and human health, with immediate improvements to indoor air quality (IAQ) becoming a priority.

Volatile organic compounds (VOCs) are a class of contaminants found in indoor and outdoor environments. Among the most studied VOCs in indoor environments are formaldehyde, acetaldehyde, benzene, toluene, glycol ethers, alpha-pinene, limonene, methyl ethyl ketone (MEK), methanol, acetic acid, and formic acid (Rovelli et al., 2019; Missia et al., 2010). In addition to moving from the outside to internal spaces, these pollutants are also produced during inhabitants' activities, such as cooking, cleaning (Steinemann, 2015), and smoking (Justo Alonso et al., 2022); moreover, they can be released from building materials or furniture (Kim et al., 2006), even if the increasing use of new and green construction and decorative materials has significantly decreased the emissions of typical indoor VOCs. On the other hand, while the materials used in interiors are becoming less emissive, indoor environments are growing increasingly more airtight, with reduced air exchange, in order to minimize heat loss; this is no longer the case only in winter but also occurs in summer due to the generalized increase in temperatures.

Normally, carbon dioxide (CO₂) is non-toxic; however, in crowded and poorly ventilated rooms, it can lower the IAQ and it has been associated with sick building syndrome (SBS). The American Society of Heating, Refrigeration, and Air Conditioning Engineers (ASHRAE) currently recommends that indoor CO₂ levels should be maintained below 1000 ppm; however, this value is often exceeded. For example in the literature there are evidences that CO₂ levels in two schools located in Italy reached up to 5136 ppm in classrooms where the windows were closed during lessons (Schibuola and Tambani, 2021). In a study of 10 classrooms in Australia, the average CO₂ levels ranged between 657 ppm and 2235 ppm, and the maximum values for CO₂ concentrations ranged from 3799 ppm to 5000 ppm; these values were recorded in three classes during school hours (Andamon et al., 2023).

The use of proper heating, ventilation, and air-conditioning systems (HVAC) constitutes a key strategy for improving IAQ; however, these systems consume half or more than half of domestic and non-domestic buildings' electrical energy (Pérez-Lombard et al., 2008). On the other hand, the relatively recent, but quickly increasing, interest in CO₂ capture as a strategy for global warming control is paving the way for the development of materials suitable for CO₂ adsorption techniques.

A number of studies have been carried out to analyze the air pollutants and its negative impact not only on human's health and the environment but also on buildings, historical monuments, cultural heritage objects and artworks (Silva et al., 2020b; Oliveira et al., 2020; Silva et al., 2020c; Grøntoft et al., 2011; Grøntoft and Marincas, 2018). For this reason, many strategies have been developed to counteract the issues related to poor air quality. As a flexible, inexpensive, efficient, and simple method, adsorption can be used in the removal of air pollutants

that are produced by various activities. The most extensively used and popular adsorbents are carbonaceous materials, such as carbon nanotubes, graphene, carbonaceous nanofiber membranes, or activated carbon with a high specific surface area and a microporous structure. However, the main issue present throughout the entire process of producing these materials is the use of nonrenewable precursors, such as petroleum residues, coal, peat, and lignite, which are associated with high costs and extensive energy consumption (Lapuerta et al., 2008). Typical everyday waste materials, especially those lignocellulosic ones, such as agricultural byproducts, food waste, and industrial byproducts, are potential precursors of activated carbon (Streit et al., 2021; Kerkhoff et al., 2021; Pigatto et al., 2020; Salomón et al., 2021; Lazarotto et al., 2021; Georgin et al., 2021; Sellaoui et al., 2021). Furthermore, these materials necessitate the development of an environmentally friendly method of reducing the problems related to their disposal. These low-cost feedstocks are ideal candidates for production of activated carbon which need to be very easily accessible to facilitate the scaling up of the process. Different biomass wastes have been studied as potential precursors of porous carbon. For example, bamboo chips (Liu et al., 2022), wheat straw (Zhang et al., 2022), potato peels (Bernardo et al., 2016), argan nutshells (Mokhati et al., 2021), orange peels (Pandiarajan et al., 2018), banana peels (Singh et al., 2018), coffee grounds (Wen et al., 2019), olive stones (Hazzaa and Hussein, 2015), and other byproducts have been successfully carbonized and activated for use in removing various water and air pollutants.

In this work, coffee grounds and olive stones were chosen as precursors of porous carbons. Coffee is one of the most widely consumed beverages worldwide, with more than five million tons of it produced annually (International Coffee Organization, 2022). Typically, coffee grounds and other organic waste are composted, burned, or, in the worst-case scenario, end up in the landfill. Alternative ways of using waste coffee grounds on an industrial scale include, for example, transforming them into biofuel, biodiesel, bioethanol, or biomaterials.

In 2022–2023, around 1.5 million tons of olive oil was produced by the leading producers of olive oil in Europe (Spain, Italy, Greece, and Portugal) (European Commission, 2023). Due to its range of different valuable properties, it is used in gastronomy, cosmetics, and pharmaceuticals. However, the process of manufacturing olive oil is also related to the generation of large amounts of waste and byproducts such as leaves, olive mill wastewater (OMW), and olive mill solid wastes (OMSW), i.e., olive stones, olive mill husks, olive cakes, and pomace.

Both selected precursors, coffee grounds and OMSW like olive stones, are rich in cellulose, hemicellulose, and lignin (Ballesteros et al., 2014; Valvez et al., 2021), which makes them other potential precursors for activated carbon.

In general, there are three different processes for the preparation of activated carbon: physical activation, chemical activation or the combination of both. In the first case, the raw precursor is carbonized, and then simultaneously activated (single-step process) or the obtained char from the carbonization step is collected and subsequently submitted to activation (two-step process) by using oxidizing gases like carbon dioxide (Singh et al., 2017), or steam (Kishibayev et al., 2021), among others.

Chemical activation consists of a single-step process, where the raw carbonaceous material is first mixed or impregnated with the chemical agent. Frequently used activating agents are classified as bases such as KOH and NaOH (Serafin et al., 2023), acids like H₃PO₄ (Bedoui et al., 2021) and H₂SO₄, or even salts such as K₂CO₃ and ZnCl₂ (Hayashi et al., 2002), followed by heating in an inert atmosphere. After cooling, the obtained product is rinsed with distilled water or mild acid to remove the remaining activating agent.

Many activating agents like alkali hydroxides are hazardous, expensive and corrosive (Singh et al., 2023), while ZnCl₂ is unfriendly to the environment and may create waste disposal problem, which makes difficult to implement production on the industrial scale. For this reason, K₂CO₃ has been proposed as an eco-friendly activating agent (Sevilla

et al., 2021; Lobato-Peralta et al., 2022; Adinata et al., 2007). Moreover, activated carbon obtained by K_2CO_3 activation is normally rich in micro- and narrow pores, and increases the carbon yield (comparing to the one obtained by KOH) (Mestre et al., 2014; Mestre et al., 2019), which increases its potential for production on a larger scale.

To the best of our knowledge, no previous study of activated carbons derived from coffee grounds and olive stones being used for VOCs adsorption in low concentrations, simulating the indoor pollutants concentrations, has been reported; therefore, the present work intends to fulfill this gap. Additionally, the ability to conduct CO_2 capture is evaluated to expand IAQ control.

Our work focused on the following aspects:

- The valorization of food byproducts, i.e. spent coffee grounds and olive stones from businesses at a local scale;
- The repurposing of these byproducts as green, feasible, eco-friendly, and low-cost valuable porous products with a high specific surface area;
- The optimization of process conditions (e.g., the type of activator, type and time of activation);
- Testing the adsorption properties of the obtained biomass-derived carbons and comparing their performance to that of commercially available activated carbon.

This study demonstrates the first step of producing activated carbon, and future studies will focus on selecting the best source of activated carbon and using it for further research focused on producing innovative filters for improving IAQ. To achieve this goal, different process approaches were studied. Waste coffee grounds and olive stones were used as precursors of biochar and activated carbons. The influence of different activation methods, with and without a previous pyrolysis step, on the development of the textural and chemical properties of the produced samples was studied. We assessed the performance of the biochars and activated carbon samples, when applied to the adsorption of MEK and toluene as model pollutants, in concentrations lower than the threshold limits. In addition, a further objective of this study is to evaluate the performance of the produced samples in CO_2 capture.

2. Materials and methods

2.1. Characterization of biomass precursors

Around 500 g of waste coffee grounds (CG) were collected from a cafeteria located in Senigallia (Italy). Open-air pre-drying was conducted, and then the samples were oven-dried at $50\text{ }^\circ\text{C}$ for 8 h. In the next step, all coffee grounds were sieved until the material passed $500\text{ }\mu\text{m}$. An olive mill located in the Alentejo region of Portugal provided 1 kg of crushed olive stones (OS) with a diameter of 2–3 mm; the stones were then dried at $50\text{ }^\circ\text{C}$ for 8 h.

Morphological and elemental analyses were conducted via a scanning electron microscope (ZEISS SUPRA 40) equipped with an energy-dispersive X-ray spectroscope (Bruker Quantax 200-Z10). To determine the thermal stability of the raw material, thermogravimetric (TGA/DTG) analysis was undertaken from $25\text{ }^\circ\text{C}$ to $1000\text{ }^\circ\text{C}$ under an inert atmosphere with a heating rate of $10\text{ }^\circ\text{C}/\text{min}$ flow of N_2 using a TGA/SDTA851 (Mettler Toledo) instrument. Similar analytical procedures were reported by several adsorption studies (Allahkarami et al., 2023; Grassi et al., 2022; Nascimento et al., 2023; Pereira et al., 2023).

The obtained carbonaceous materials were compared to the commercial activated carbon Carbosorb PCF (COMELT S.p.A), produced via the physical activation of selected vegetable raw material; a surface area of $1200\text{ m}^2/\text{g}$ is declared on the technical datasheet, as well as a particle size from 20 to $250\text{ }\mu\text{m}$. It is labelled as AC-COM.

2.2. Process of synthesizing biomass-derived carbons

The biomass-derived carbons were prepared from olive stones and coffee grounds via the chemical activation method, using potassium carbonate (K_2CO_3) as an activation agent, and through the physical activation method using CO_2 as an activation agent. Briefly, the carbonization/activation experiments were conducted in a lab-scale pyrolysis reactor of tubular design with the following dimensions: an outer diameter of 2.5 cm and a length of 50 cm. The quartz reactor was placed in the electric vertical (in the case of physical activation) or horizontal (in the case of chemical activation) tube furnace (Resiprel Lda) controlled by a PID programmable temperature controller (RKC, REX—P96). Since an inert environment is required for the pyrolytic process, nitrogen (N_2) flow was supplied throughout the entire process and the gas flow was controlled by an Omega flow meter. Carbon samples were obtained as follows:

- Via chemical activation: each type of biomass, CG or OS, was mixed with K_2CO_3 at a mass ratio of 1:3 (Galhetas et al., 2014). This ratio was selected to increase the contact area between the precursor and the activating agent (Li et al., 2016). The prepared mixture was transferred to the reactor and heated up to $800\text{ }^\circ\text{C}$ at a heating rate of $10\text{ }^\circ\text{C}/\text{min}$ in a flowing stream of N_2 ($150\text{ ml}/\text{min}$), shown as Step I in Fig. 1. The chemical activation process for coffee grounds and olive stones. The activation process was maintained for 1 h (Step II). After cooling, the obtained product was washed with distilled water until the washing water presented a pH of around 5.7 (the same pH value of the deionized water used for the washing). The as-prepared activated carbon was oven-dried at $105\text{ }^\circ\text{C}$ for 24 h. The obtained samples were labelled as follows: AC- K_2CO_3 -CG and AC- K_2CO_3 -OS
- Via physical activation: 10 g of biomass was placed into the reactor and heated at $5\text{ }^\circ\text{C}/\text{min}$ under an N_2 flow of $150\text{ ml}/\text{min}$ (Step I in Fig. 2). After reaching $500\text{ }^\circ\text{C}$, the temperature was kept constant to facilitate the pyrolysis (carbonization) process for 1 h (Step II). In Step III, the temperature was raised to $800\text{ }^\circ\text{C}$ at a heating rate of $10\text{ }^\circ\text{C}/\text{min}$. After reaching $800\text{ }^\circ\text{C}$, the N_2 flow was stopped, and the CO_2 was turned on with a flow of $100\text{ ml}/\text{min}$ (Step IV). The activation process lasted from 1 to 2 h in the case of coffee grounds (Fig. 2a) and for 3 h in the case of olive stones (Fig. 2b). After that, CO_2 was changed again to N_2 until room temperature was reached. The obtained samples were labelled AC- CO_2 (1 h)-CG and AC- CO_2 (2 h)-CG for the coffee grounds and AC- CO_2 -OS for the olive stones.
- Without activation: to study the influence of the activation on one of the precursors, coffee grounds were subjected to the carbonization process at $500\text{ }^\circ\text{C}$ with retention times of 15 min and 2 h, without any

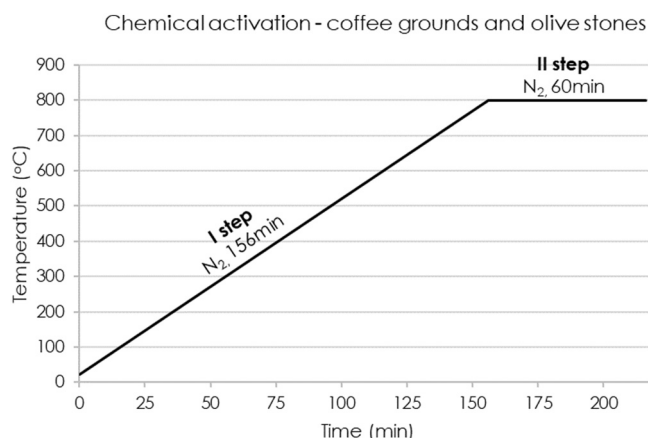


Fig. 1. The chemical activation process for coffee grounds and olive stones.

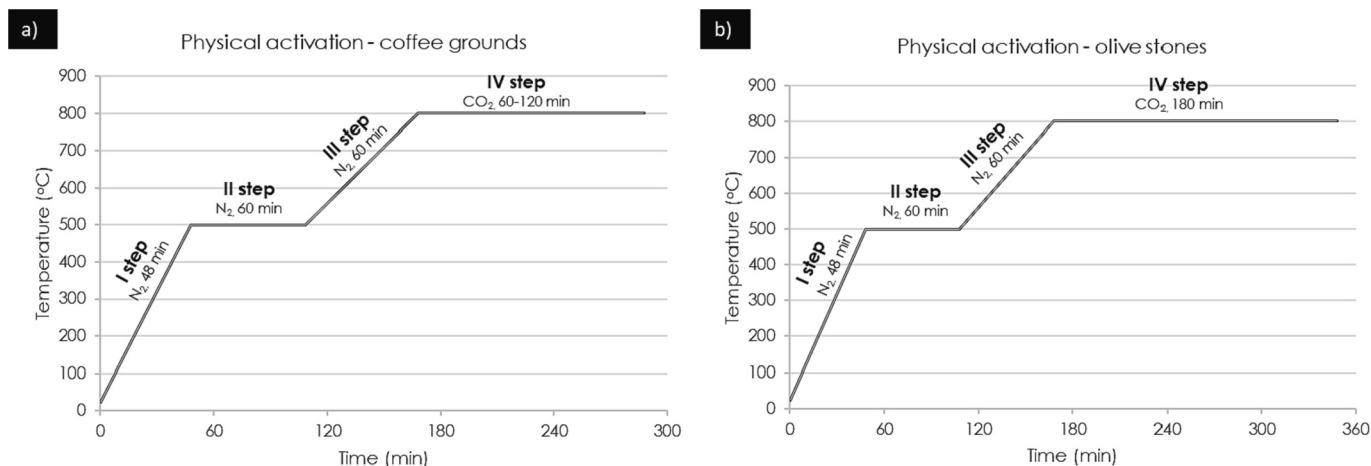


Fig. 2. The physical activation process of a) coffee grounds and b) olive stones.

further activation steps, as shown in Fig. 3. These products were referred to as B-(15')-CG and B-(2 h)-CG.

All the prepared samples were sieved again and milled until the material passed 500 μm ; they were then kept in air-tight containers at room temperature (20 $^{\circ}\text{C}$). The preparation conditions of all biomass-derived carbons used in this study are summarized in Table 1.

The yield (%) of each sample, which is defined as the weight of the final product divided by the mass of the raw material (Diao et al., 2002), was calculated using Eq. (1):

$$\text{Yield (\%)} = \frac{W_0}{W_p} * 100 \quad (1)$$

where W_0 , is the mass of the raw material and W_p is the mass of the sample at the end of the process.

2.3. Biomass-derived carbons characterization

Morphological and elemental analyses of the biomass-derived carbons were carried out using a scanning electron microscope (SEM) at the optimum operating condition with 1000-magnification, at an excitation energy of 10 kV, along with energy-dispersive X-ray spectroscopy (EDS) analysis. Textural properties including the specific surface area (SSA) were determined using the Brunauer–Emmett–Teller (BET) equation, the total pore volume (V_{total}) was determined by the amount of N₂ adsorbed at $P/P_0 = 0.95$, the micropore volume (V_{micro}) was determined using the t-plot method, and the mesopore volume (V_{meso}) was

determined by the difference between V_{total} and V_{micro} of the obtained samples; the above metrics were retrieved from the N₂ adsorption–desorption isotherms at -196°C (77 K) using ASAP 2010 Micromeritics equipment. CO₂ adsorption–desorption isotherms (Anton Paar Quantachrome Instruments, Boynton Beach, FL, USA) were obtained to characterize the narrowest pores at 0 $^{\circ}\text{C}$ (273 K) using Automated Gas Sorption Data software. The surface area and pore size were evaluated according to the DFT model. Pore size distributions and the average pore diameter were obtained by applying the non-local density functional theory (NLDFT) and DFT methods to the N₂ and CO₂ adsorption data. Before analysis, the samples were degassed under a vacuum for 12 h at 150 $^{\circ}\text{C}$. CO₂ adsorption–desorption isotherms within the relative pressure (P/P_0) range from 0 to 0.03 were collected to evaluate CO₂ uptake.

X-ray diffraction analysis was performed on the carbons to determine the degree of crystallinity or amorphousness of the samples. In this case, the measurements were performed using a Bruker AXS D8 Advance instrument at an angle of diffraction (2θ) between 10 $^{\circ}$ and 60 $^{\circ}$, with the radiation source Cu- α having a wavelength $\lambda = 1.5406 \text{ \AA}$, an operating voltage of 40 kV (current of 40 mA), step = 0.02, and scan speed = 2 s/step at room temperature.

Ash, fixed carbon, and moisture content in the obtained samples were analyzed via thermogravimetric analysis, according to the ASTM Standard Test Method for Compositional Analysis by Thermogravimetry (E 1131–08), with slight modifications. The analysis was conducted on a Mettler Toledo TGA/SDTA 851 instrument, with a heating rate of 10 $^{\circ}\text{C}/\text{min}$ from room temperature to 900 $^{\circ}\text{C}$ under a N₂ atmosphere (20 ml/min). About 10 mg of the sample was heated from room temperature at 25 $^{\circ}\text{C}$ to 110 $^{\circ}\text{C}$ in N₂ and held isothermally at 110 $^{\circ}\text{C}$ for 10 min, until complete dehydration was accomplished. The temperature was then raised to 900 $^{\circ}\text{C}$ and held isothermally for 10 min to determine the quantity of volatile matter. The atmosphere was then changed to an oxidizing one to create the environment for combustion; this temperature was held for 30 min until the sample's weight remained unchanged. The weight lost during this period was due to the reaction of the fixed carbon with oxygen, and the remaining residue was ash.

The surface chemistry of the activated carbon sample was characterized via the determination of the pH at the point of zero charge (pH_{PZC}) according to the reverse mass titration method proposed by Noh and Schwarz (Noh and Schwarz, 1989).

Fourier transform infrared (FT-IR) spectroscopy was used to study the molecular structure of the raw biomass (precursor) and obtained biomass-derived carbons in transmission mode using a Perkin Elmer FT-IR spectrometer according to the following procedure: 1 mg of the dried sample was mixed with 50 mg of KBr powder and the mixture was pressed into pellets (around 1 cm in diameter) under 8 tons of pressure for 2 min, and the product was then used for analysis (Cuhadaroglu and

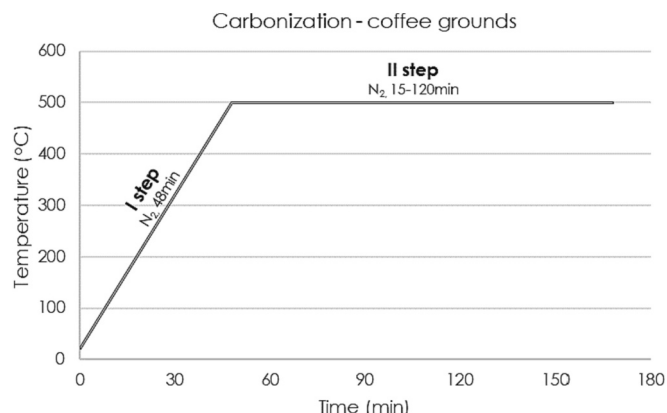


Fig. 3. Process of carbonizing coffee grounds.

Table 1
List of prepared samples (biomass-derived carbons) and experimental conditions.

Sample name	Type of precursor	Type of activation	Activation time (h)	Process time ^a (min)	Activation or Carbonization temperature (°C)
AC-K ₂ CO ₃ -CG	Coffee grounds	Chemical	1	216	800
AC-K ₂ CO ₃ -OS	Olive stones	Chemical	1	216	800
AC-CO ₂ -OS	Olive stones	Physical	3	348	800
AC-CO ₂ (2 h)-CG	Coffee grounds	Physical	2	288	800
AC-CO ₂ (1 h)-CG	Coffee grounds	Physical	1	228	800
B-(2 h)-CG	Coffee grounds	–	–	168	500
B-(15)-CG	Coffee grounds	–	–	63	500

^a Time considered from the beginning of heating up to the end of the pyrolysis or activation process.

Uygun, 2008). The FT-IR spectra were recorded between 4000 cm⁻¹ and 450 cm⁻¹, with a spectral resolution of 4 cm⁻¹ and 32 scans.

2.4. VOCs adsorption

The VOCs adsorption properties of each sample were tested at a controlled temperature (20 ± 2 °C) and a relative humidity (RH) of 50 ± 5%. To ensure that all the samples had a homogeneous distribution of sorbent, a fixed mass of 0.05 g was first mixed with 5 ml of distilled water in a beaker and placed in the ultrasound bath. After 5 min, the mixture was poured into a Petri dish and the beaker was washed with an additional 2 ml of water to make sure that all content had been transferred; it was then placed in the oven at 105 °C for 12 h. The depolluting properties were evaluated in terms of the adsorbent properties in the chamber as a batch reactor, according to the modified method used in previous works (Palmieri et al., 2020; Maqbool et al., 2022; Giosuè et al., 2023). Briefly, after cooling at room temperature, each sample was placed on the sample holder in the 17 l sealed glass chamber. Two different types of liquid solvents were used as pollutant models: methyl-ethyl-ketone (MEK) and toluene. A fan was placed in the bottom of the reactor to guarantee continuous air recirculation. Then, 1 µl of one type of VOC was injected into the reactor with a micro-syringe to ensure an initial concentration of 16 ppm (± 1 ppm) for MEK and 14 ppm (± 1 ppm) for toluene, after evaporation. To monitor changes in the VOCs concentration over time, a photoionization detector (PID) (Aeroqual, Series 900, 0–30 ppm range) was used. A blank test was performed before each analysis to control the concentration during the analysis. Fig. 4 and Fig. S3 in the supplementary materials illustrate the experiment setup used for the static adsorption test. Table 1 lists the physical properties and the acceptable concentration limits of the adsorbates used in this work.

The percentage of each adsorbed VOC was calculated according to the difference between the concentrations after 90 min of monitoring (C_t) and the concentration recorded at the beginning of the test (C₀) according to Eq. (2):

$$\text{VOC adsorbed (\%)} = \frac{C_t - C_0}{C_t} \times 100 \quad (2)$$

The value of VOCs uptake (mg/g) after 90 min is determined using Eq. (3) (Abdul Manap et al., 2018):

$$qe = \frac{C_0 - C_e}{W} \times V \quad (3)$$

where C₀ (ppm) is the initial gas phase concentration of MEK or toluene and C_e (ppm) is the gas phase concentration of MEK or toluene at equilibrium; V is the interior volume of the test chamber in liters (17 l), and W is the mass of the sample (0.05 g).

2.5. Reusability

The reusability of the samples was evaluated after their exposure to VOCs for 90 min (Cycle I). The used samples were dried at 100 °C for 1 h and then reused to assess their performance (Cycle II).

3. Results and discussion

3.1. Characterization of precursors and carbon samples

3.1.1. Thermogravimetric analysis

Fig. 5 shows the evolution of the sample mass (TGA) and its derivative (DTG) over time during the pyrolysis of CG and OS under inert conditions (N₂).

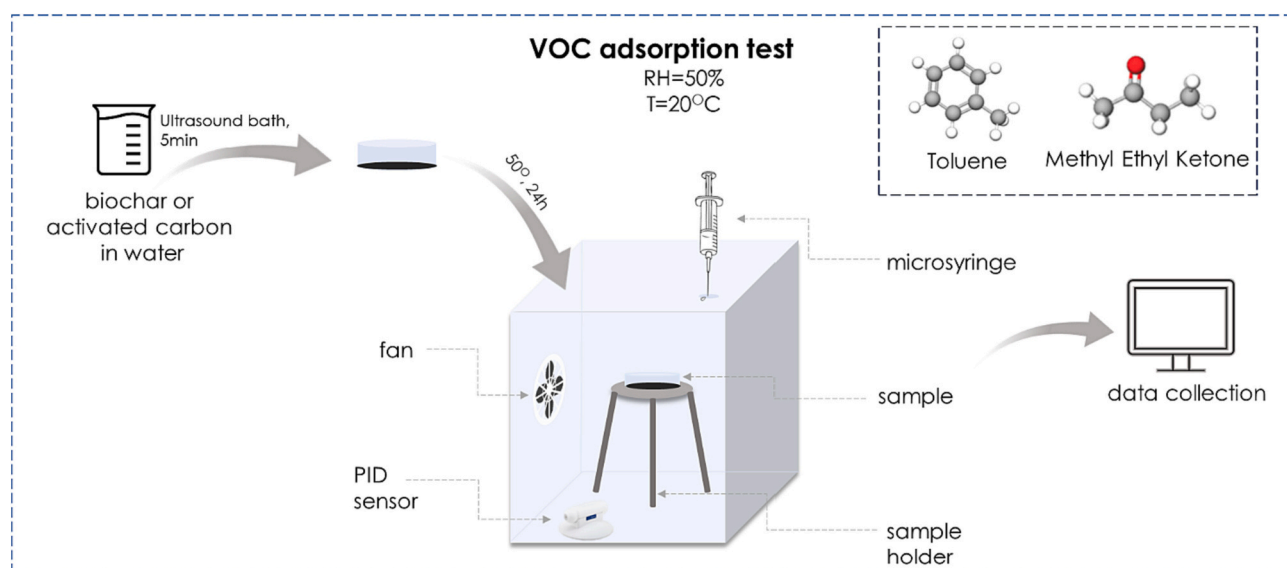


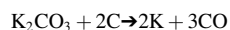
Fig. 4. Experimental chamber for VOC adsorption.

The thermal degradation can be divided into three (in the case of OS) and four (in the case of GC) regions. Both TGA curves of coffee grounds and olive stones first present a mass loss of around 10 % up to 150 °C, which is related to the loss of moisture and highly volatile organic compounds (Sanginés et al., 2015). Two peaks in the DTG plot of the olive stones, with the maxima at 276 °C and 324 °C, and two peaks in the DTG plot of coffee grounds at 304 °C and 346 °C represent the degradation of hemicellulose and cellulose, respectively. As previously reported, hemicellulose mainly decomposes at 220–315 °C, and cellulose mainly decomposes at 315–400 °C (Liu et al., 2014). The simultaneous degradation of lignin, the third main component of the biomass, occurred in the temperature range of 160–900 °C (Liu et al., 2014; Hongqiang et al., 2014) with the maximum peak at 391 °C representing the fourth degradation region of the coffee grounds. The devolatilization of biomasses is related to the differences in the elemental and chemical compositions of the two samples. Under higher temperatures, the material is quite stable, with not significant loss of mass (3 %) corresponding to the loss of oxygen molecules. The following results provide insight into the carbonization temperature range required for the production of activated carbon and indicate that 800 °C is sufficient to completely remove the volatile matter, as, after 500 °C, both materials show only slight weight loss, as also reported in (Bedoui et al., 2021; Park et al., 2016).

3.1.2. Morphology and elemental analysis

Fig. 6 shows SEM pictures of coffee grounds, olive stones, biochars, and activated carbons. Coffee grounds (Fig. 6a) and olive stones (Fig. 6h) have a bulky morphology with a rather smooth surface and no pores. After the thermal treatment, there was a change in the morphology in all the samples, and a porous structure featuring large cavities with an entrance of several micrometers was formed, exhibiting a heterogeneous structure. These cavities result from the reaction of activating agents and carbon atoms in the precursors (Laksaci et al., 2017) and serve as channels, allowing the molecules of the adsorbate to reach pores located in the interior of the carbon (Foster et al., 1992). In the case of olive stones, the structure is characterized by a thick wall structure with rough edges (Hazzaa and Hussein, 2015). The pore dimensions of AC-K₂CO₃-CG, shown in Fig. 6d and Fig. 6e, are smaller than those of the rest of the carbon samples. As a result, an increasing number of activating agents causes the structure to exhibit a merging of the micropores and the development of mesopores, which was also observed previously in (Gundogdu et al., 2013).

It was reported that, after dispersion on the surface, K₂CO₃ undergoes crosslinking condensation reactions with the cellulosic internal structure of the precursor in an inert environment above 600 °C, leaving the non-penetrating pores (Hayashi et al., 2002). According to the reported literature, the associated reaction is presented as follows:



The metallic potassium could further develop porosity via intercalation through carbon sheets to enlarge the pores (Zhu et al., 2018).

In contrast, during physical activation, at high temperatures, carbon atoms and CO₂ activator form CO + H₂ or CO to form a porous structure (Li et al., 2020).

Table S1 in the supplementary materials summarizes the elemental analysis and O/C atomic ratios of all the samples. Fig. 7a shows the main elements contained in the samples, selected from those detected via EDX (C, O, Mg, K, S, Ca, P). As expected, carbon and oxygen are the main elements of the biomass precursors composed of lignocellulosic components. Both types of biomasses have high carbon content, at approximately 60 %. After pyrolysis and activation, the carbon content increases to 80–90 % and the content of oxygen decreases from 41–45 to 10–14 %. The activation time did not significantly affect the carbon content (differences between 3 and 7 % are considered negligible). The highest carbon content characterizes AC-K₂CO₃-CG (88.89 %) and AC-K₂CO₃-OS (88.74 %), while the lowest was obtained for biochar B-2 h-CG (82.11 %). The atomic ratio O/C was used to evaluate the hydrophilicity and polarity of the carbons, which, after carbonization and activation, decreased from 0.51–0.54 O/C to 0.08–0.12 O/C, indicating the successful removal of oxygen-containing functional groups and the hydrophobic nature of the produced carbonaceous samples. The low potassium content in the chemically activated carbons, which was comparable to other samples, indicates sufficient washing. Fig. 7b clearly shows that, after activation and with the increasing duration of the process, the carbon content slightly increases; however, when comparing all the activated samples, the process time exhibits no dependence on the carbon content.

3.1.3. Yield and proximate analysis

From the industrial point of view, it is important to evaluate the carbon yield to determine whether the material is feasible for large-scale applications. The mass yields of the obtained samples (Table 3) ranged from 17 % to 30 %. An increase in the pyrolysis time from 15 min to 2 h decreased the yield of the product from 28 % to 24 %. These values are similar to those previously obtained (Vardon et al., 2013) from the pyrolysis of coffee grounds at 450 °C and a retention time of 2 h. Despite the use of different precursors, the duration of physical activation did not influence the product yield of the activated carbon samples, which ranged from 20 % to 21 %. In this work, the highest product yield was observed when using the chemical activation of olive stones as a precursor (30 %); comparing it to biochar samples with similar yields indicates that the activation exerted a slight influence. This conclusion was also confirmed by other authors (Sanginés et al., 2015), who proved

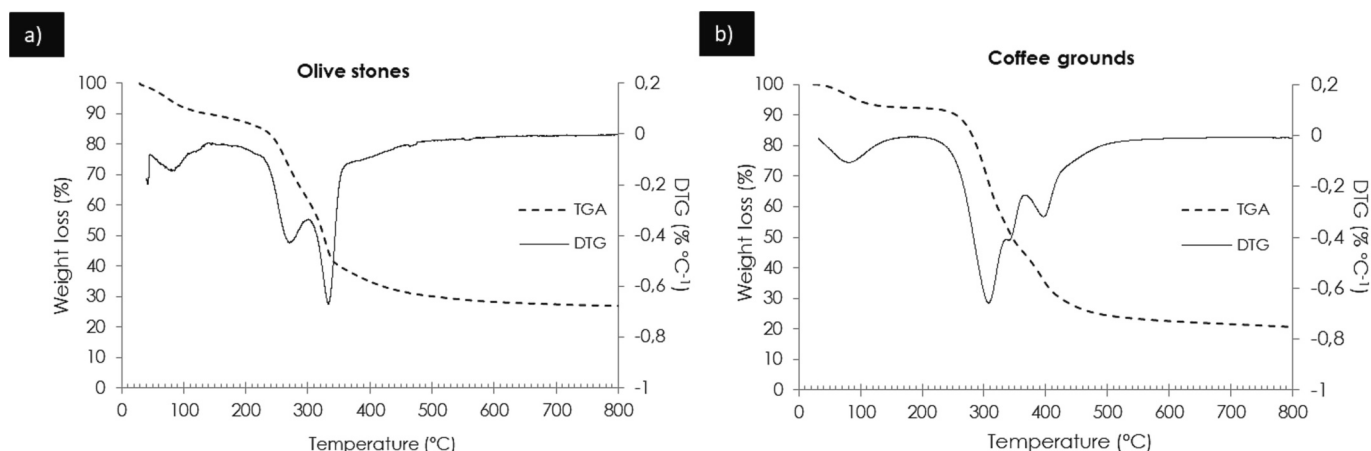


Fig. 5. Thermogravimetric analysis (TGA) and differential thermogravimetry (DTG) curves of (a) olive stones and (b) coffee grounds.

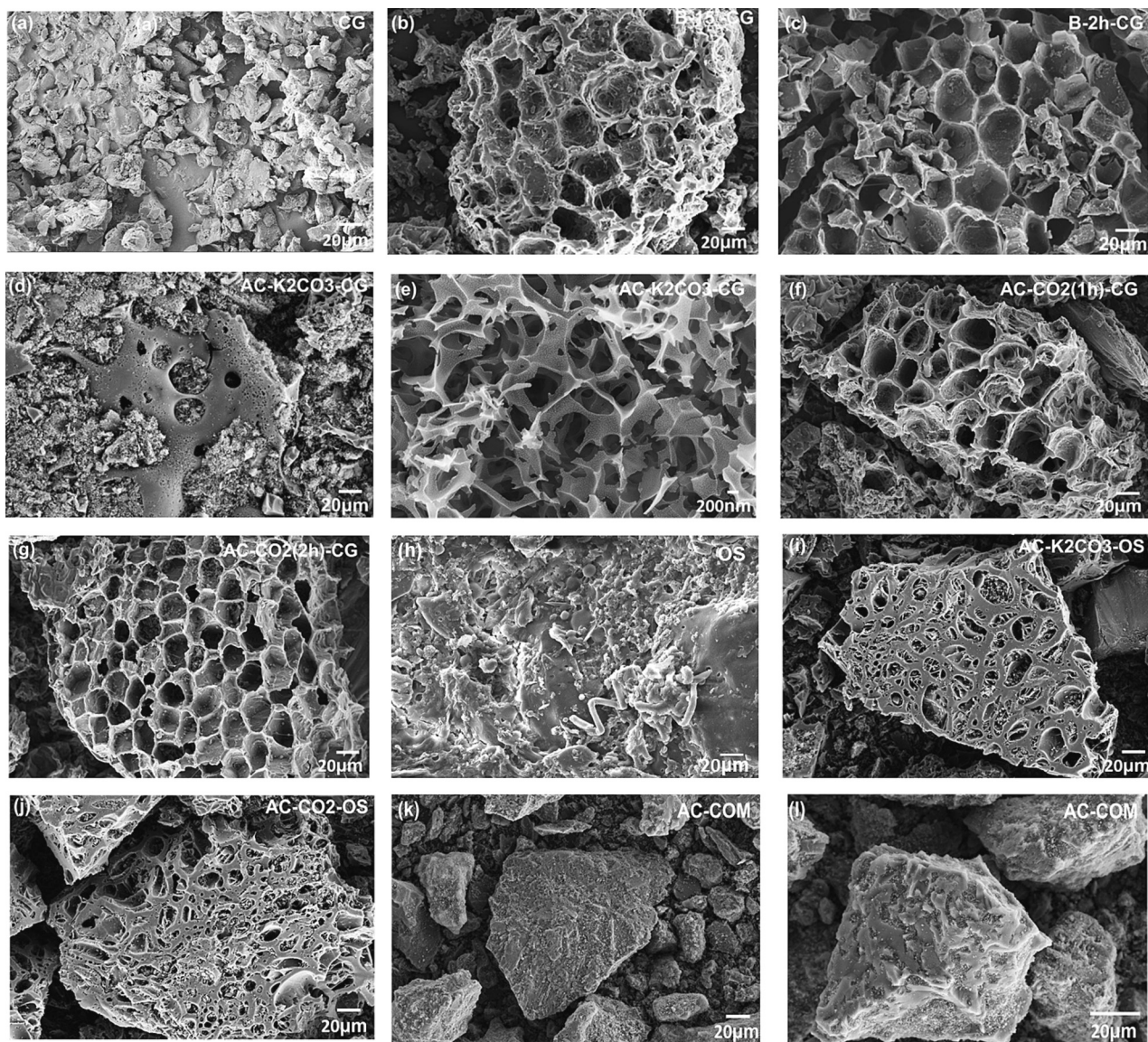


Fig. 6. SEM images of (a) CG, (b) and (c) CG—biochars, (d) and (e) CG after chemical activation, (f) and (g) CG after physical activation; (h) OS, (i) OS after chemical activation, and (j) OS after physical activation; (k) and (l) commercial activated carbon at MAG 1.00Kx.

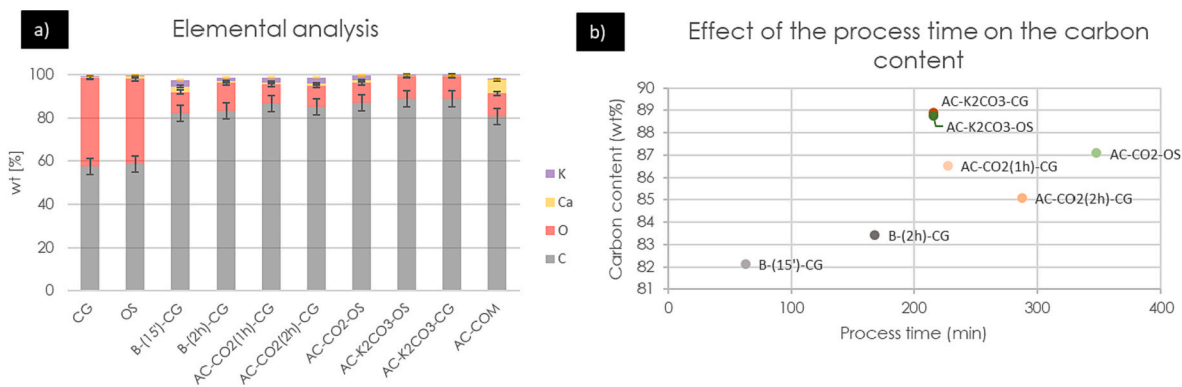


Fig. 7. Elemental analysis (a) and (b) effect of the process time on the carbon content.

that the solid fraction (biochar) is reduced rapidly during the initial stages of the pyrolysis process (between 200 °C and 400 °C) while the quantity of gas and oil increases, and the application of higher

temperatures resulted in a progressive but less significant reduction in the solid fraction. The same precursor, when activated by physical activation, resulted in a 9 % lower product yield (21 %). In case of coffee

grounds, the yields of the product obtained from the activation via both methods were similar: 17 % in the case of chemical activation and 20 % in the case of physical activation.

The proximate analysis data collected in Table 3 show the high volatile fraction of the precursors (77 %–78 %), which was significantly reduced after pyrolysis (28 %–35 %), chemical (18 %–19 %), and physical (16 %–23 %) activations. The key parameters influenced by the volatile matter content were the temperature and process time. The lowest volatile matter content was found in AC-CO₂-OS, which was produced over the longest process time (three hours). Increasing the duration of carbonization would release the volatile compounds that were still left. On the other hand, after the thermal treatment, the fixed carbon content increased from 12 %–14 % to 56 %–69 %. The experimental data also show that, as a result of volatile matter release, the ash content of the CG-derived carbons increased from 0.6 % to 5.7 %, but, after chemical activation, it was only two times higher. This difference in ash content was much lower in the case of the OS-derived samples that underwent chemical (1.6 %) and physical (0.9 %) activation and raw olive stones (0.6 %). A high ash content was observed in the biochar samples (4.1 %–4.5 %) and physically activated carbons (5.6 %–5.7 %), since no washing was performed on the resulting carbons.

pH_{pzc} is the parameter that indicates inherent acidic or basic nature of the carbon sample and the degree of oxidation. After chemical activation, the samples (AC-K₂CO₃-CG and AC-K₂CO₃-OS) exhibit a neutral character. Meanwhile, the samples that underwent physical activation, as well as the biochars, show significantly alkaline characteristics; this is mainly related to their higher ash content.

3.1.4. Textural properties

Table 4 summarizes the textural properties of the samples. The SSA and V_{total} followed the pattern of AC-K₂CO₃-CG > AC-CO₂-OS > AC-K₂CO₃-OS > AC-CO₂(2 h)-CG. As expected, the use of a chemical activation process led to the development of higher porosity (Dias et al., 2007), indicating that K₂CO₃ is a more effective activating agent than CO₂, and these samples resulted in a higher surface area. The activation via K₂CO₃ does not have the same effect on the two biomasses, being much more effective for coffee grounds that exhibit the highest surface area of 1597 m²/g and the highest total pore volume of 0.736 cm³/g. However, as reported by Hayashi and coauthors (Hayashi et al., 2002), the structure of carbon depends on the precursor used in the production process. K₂CO₃ is reduced more easily by disorganized carbon than by crystallite carbon. Consequently, it can be assumed that coffee grounds have a less crystalline structure, so that K₂CO₃ was able to remove more carbon as CO gas, leading to the formation of a higher specific surface area. This hypothesis was later confirmed by the XRD spectra shown in Fig. 9.

All the materials possess significant micropore content, ranging from 79 to 80 % for the chemically activated carbons and 82–92 % for the physically activated carbons. On the other hand, the biochars (B-(2 h)-CG and B-(15')-CG) appeared to be non-porous or microporous materials due to very low amounts of adsorbed N₂. Adsorption and desorption isotherms of N₂ are shown in Fig. S4 in the supplementary materials. According to the IUPAC (International Union of Pure and Applied Chemistry) classification, all the isotherms exhibited Type I behavior, confirming a predominance of micropores (<2 nm). AC-K₂CO₃-CG features a small hysteresis loop of type H4 and low levels of deviation from the plateau region in the isotherm plots, which is related to the micro-/mesoporous structure of carbon (Thommes et al., 2015). The hysteresis loops of AC-K₂CO₃-OS, AC-CO₂(1 h)-CG, and AC-CO₂(2 h)-CG were not closed, perhaps due to the lower content of mesopores (Zhu et al., 2018). The high adsorption values occurred at a low value of relative pressure: nearly 0.1 for AC-CO₂-OS and 0.05 for the rest of the carbons. The isotherms remain nearly horizontal over a range of P/P₀, approaching unity, and the total pore volume is well defined (Lykiema et al., 1984).

The highest specific surface area (1487 m²/g) and total pore volume (0.527 cm³/g) obtained from CO₂ adsorption were exhibited by AC-

K₂CO₃-CG, followed by AC-K₂CO₃-OS, AC-CO₂-OS, AC-CO₂(2 h)-CG, AC-CO₂(1 h)-CG, B-(2 h)-CG and B-(15')-CG, with values of 870 m²/g, 778 m²/g, 716 m²/g, 649 m²/g, 331 m²/g, and 251 m²/g, respectively. The differences in the obtained values for pore volume and specific surface area between N₂ and CO₂ adsorption result from the different kinetic diameters of the two molecules: in fact, the diameter of N₂ is 0.364 nm and of CO₂ 0.330 nm (Talakesh et al., 2012). These results indicate that the microporous carbon samples contain narrow micropores (<0.7 nm) that only CO₂ can penetrate, while nitrogen cannot access them under cryogenic conditions. On the other hand, because of the high saturation pressure of CO₂ at 273 K, low-pressure (up to atmospheric pressure) experiments are limited to the analysis of pores <1.5 nm (Mukhtar et al., 2020), hence the lower values of SSA and V_{total} of AC-K₂CO₃-CG, in which larger pores were also developed.

The type of activation had a significant effect on the specific surface area and pore structure. Compared with non-activated samples (B-(15')-CG and B-(2 h)-CG), the specific surface area of the physically and chemically activated carbons, was two to three and three to six times higher, respectively. Moreover, the curves of the pore size distribution (Fig. 8) obtained according to the DFT (density functional theory) method from N₂ (Fig. 8a) and CO₂ (Fig. 8b) adsorption indicate that most of the pores of all samples have sizes smaller than 2 nm and are located in the microporous region. Additionally, the presence of narrow pores in the range of 0.3–0.7 nm illustrates the highly tunable nature of the carbon. Samples AC-K₂CO₃-OS, AC-CO₂-OS, AC-CO₂(2 h)-CG, AC-CO₂(1 h)-CG, B-(2 h)-CG, and B-(15')-CG in Fig. 8b exhibit two distinctive peaks, which indicate the presence of two pore fractions. The first is distributed between 0.30 nm and 0.45 nm and the other between 0.45 nm and 0.75 nm. Meanwhile, AC-K₂CO₃-CG is characterized by a wider pore size distribution, up to 3 nm, with the main fraction distributed between 0.45 nm and 0.75 nm.

Fig. 9 displays the XRD spectra of the carbon materials. Two broad diffraction maxima, attributed to the amorphous carbon and graphite, are demonstrated by broad peaks at 23–25° and 43–44°, corresponding to the diffraction of C (002) and C (101), respectively (Liu et al., 2010). In the case of the biochar samples (B-(2 h)-CG and B-(15')-CG), no peak was found at 43°, and, for AC-K₂CO₃-CG, AC-CO₂(1 h)-CG, and AC-CO₂(2 h)-CG, the intensity of the peak was very low. The intensity of the peak at 43° of the commercial activated carbon (AC-COM) is equal to that detected for AC-K₂CO₃-OS and A-CO₂-OS. The difference in the XRD patterns between the other samples suggests that the activation process, the time of the process, and the type of precursor affected the microcrystalline structure.

3.1.5. Chemical surface analysis

The FT-IR spectra are presented in Fig. 10 and Fig. 11, where the established functional groups contained in the coffee grounds, olive stones, and produced samples are identified. As reported in (Takada et al., 2022), due to the strong infrared absorption of carbon, the background absorption is highly significant; as such, it is quite difficult to identify the intrinsic peaks of the surface functional groups. However, it can be observed that, after carbonization and activation, the functional groups on the surface changed. The broad bands with peaks observed at approximately 3369 cm⁻¹ (for coffee grounds) and 3445 cm⁻¹ (for olive stones), which are assigned to the O–H stretching of the cellulose, absorbed water, hemicellulose, and lignin, slowly disappear during pyrolysis (biochar samples), as the pyrolysis time increases and after the chemical activation. In the case of physical activation, the intensity is much lower compared to the raw biomass. In the AC-CO₂-1 h-CG sample, the peak is in fact centered at about 3000 cm⁻¹, indicating OH groups held by intramolecular H bonds; meanwhile, in the AC-CO₂-2 h-CG sample, the peak is shifted to 3500 cm⁻¹, indicating OH groups free from H bonds. Therefore, this spectral trend is indicative of a conformational variation in molecules.

The bands at 2925 cm⁻¹ and 2855⁻¹ cm⁻¹ for CG, 2918 cm⁻¹ and 2851 cm⁻¹ for B-(15')-CG, and 2957 cm⁻¹ and 2929 cm⁻¹ for OS,

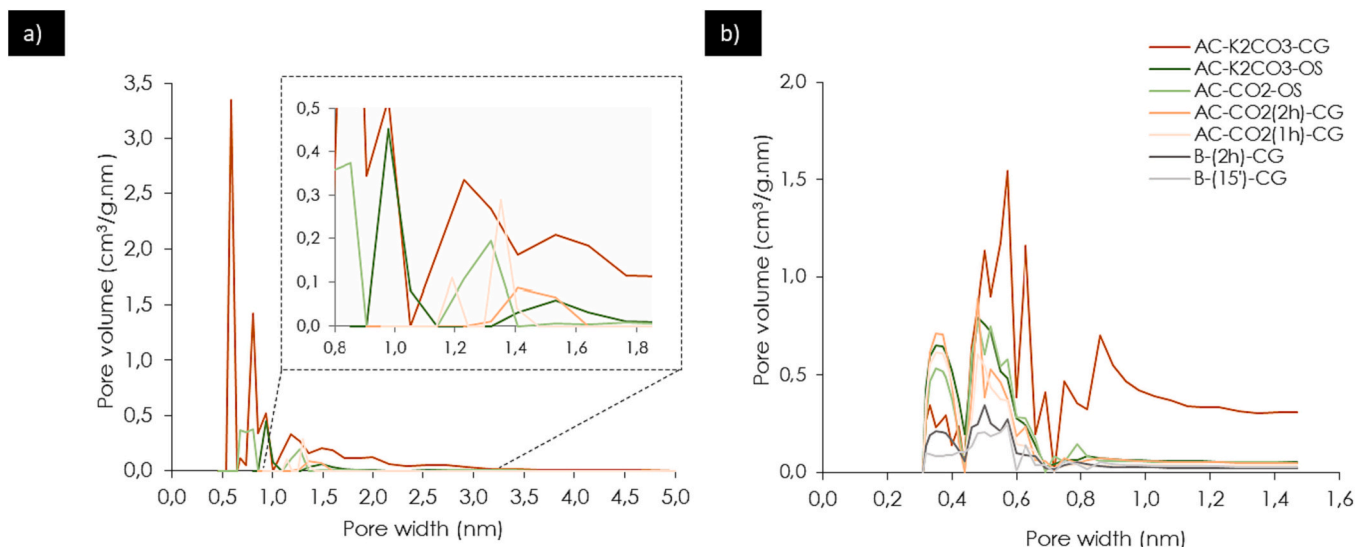


Fig. 8. The pore size distribution of the produced samples was measured with (a) N_2 and (b) CO_2 using the DFT method.

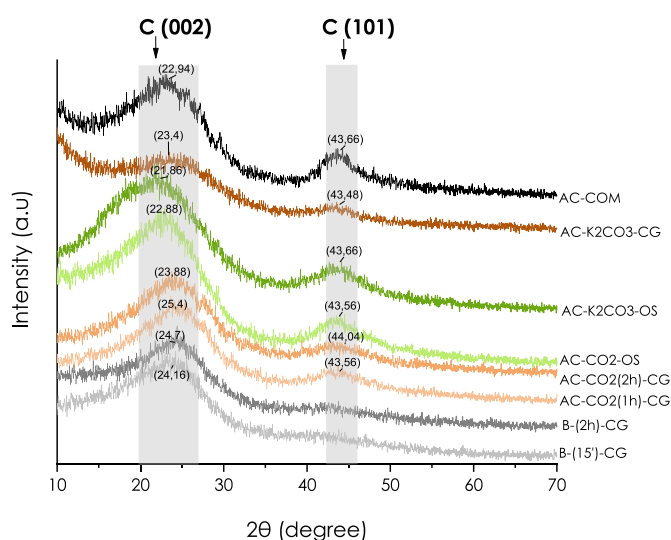


Fig. 9. XRD spectra of commercial activated carbon and of the samples obtained from olive stones and coffee grounds.

indicate the symmetric or asymmetric C—H stretching vibration of saturated aliphatic groups (alkane/alkyl) (Pérez Marín et al., 2009), which disappears after the activation step.

In the FT-IR spectra of the olive stones, the peak of the carbonyl group is at 1743 cm^{-1} and was reduced considerably after activation, almost disappearing, to be replaced by the peak at 1569 cm^{-1} ; this is prevalent in the AC- K_2CO_3 -OS and AC- CO_2 -OS samples. This spectral pattern could indicate an important structural variation in the molecule that can result from two factors: during the chemical activation, the carbonyl can be replaced by the C=N group (1569 cm^{-1}) via a reaction with an amino group, or the molecule is arranged in such a way as to expose the surface aromatic groups, clearly visible with ATR spectroscopy, rather than the carbonyl groups. The band around $1500\text{--}1700\text{ cm}^{-1}$ could also correspond to aromatic C=C stretching. Similar findings were reported by Wei et al. (Wei et al., 2023). The band around $1100\text{--}1300\text{ cm}^{-1}$ corresponds to the aromatic C—O stretching mode of C-OH and the carboxyl groups.

Moreover, small peaks at around 800 cm^{-1} , with higher values after the pyrolysis and activation processes, can be assigned to the vibration of an aromatic group and to the bending vibrations of C—H groups.

Similar spectra for activated carbon samples are commonly reported in the literature (Takada et al., 2022; Benallou Benzekri et al., 2018).

All activated carbons had similar IR transmittance spectra; however, the peak intensities were different, indicating that the produced ACs have similar surface chemical properties. Progressive changes in functional groups appear in both precursors, due to the degradation of hemicellulose, cellulose, and lignin, which are the main components of coffee grounds and olive stones. Successful aromatization caused by the decomposition and condensation of volatile matters after the carbonization and activation process (Saad et al., 2019) was also noted.

3.2. Adsorption properties

3.2.1. CO_2 adsorption

Fig. 12 presents the CO_2 adsorption–desorption isotherms of the carbon samples at $0\text{ }^\circ\text{C}$ (273 K) and under low relative pressures ($P/P_0 < 0.03$): similar conditions were applied by García-Mateos and co-authors (García-Mateos et al., 2016) and, Mochizuki and co-authors (Mochizuki et al., 2022). The desorption curves do not show hysteresis, indicating that the adsorption is fully reversible, and chemisorption does not occur. The adsorption capacities are shown in Table 5. The sequence of the highest amount of adsorbed CO_2 is AC- K_2CO_3 -CG > AC- K_2CO_3 -OS > AC- CO_2 -OS > AC- CO_2 (2 h)-CG > AC- CO_2 (1 h)-CG > B-(2 h)-CG > B-(15')-CG. These results correlate with the textural parameters. The biochar samples showed the weakest ability to adsorb CO_2 molecules because they have relatively small surface areas: $251\text{ m}^2/\text{g}$ and $351\text{ m}^2/\text{g}$ for B-(15')-CG and B-(2 h)-CG, respectively. The highest CO_2 uptake was observed for AC- K_2CO_3 -CG which has the highest surface area and micropore volume, as shown in paragraph 3.1.3; this finding highlights that a large surface area and a high micropore volume are major factors in increasing CO_2 adsorption properties.

The CO_2 adsorption capacity of AC- K_2CO_3 -CG reached 253 mg/g , value 60 % higher than that reported by (Kim, 2020), where the experimental conditions for the activated carbon samples were similar to those used in our research and the CO_2 adsorption properties were examined at $0\text{ }^\circ\text{C}$ and 0.15 bar.

A similar CO_2 uptake has been obtained (Wang et al., 2022a) where activated carbon produced via KOH impregnation reached 251 mg/g at higher pressures (1 bar). These values are aligned with those derived from the carbon material produced (Singh et al., 2017) from *Arundo donax* via KOH activation at 1 bar and 273 K , and they are slightly lower than the activated carbon obtained similarly from coffee grounds (Kim, 2020), as presented in Table 6.

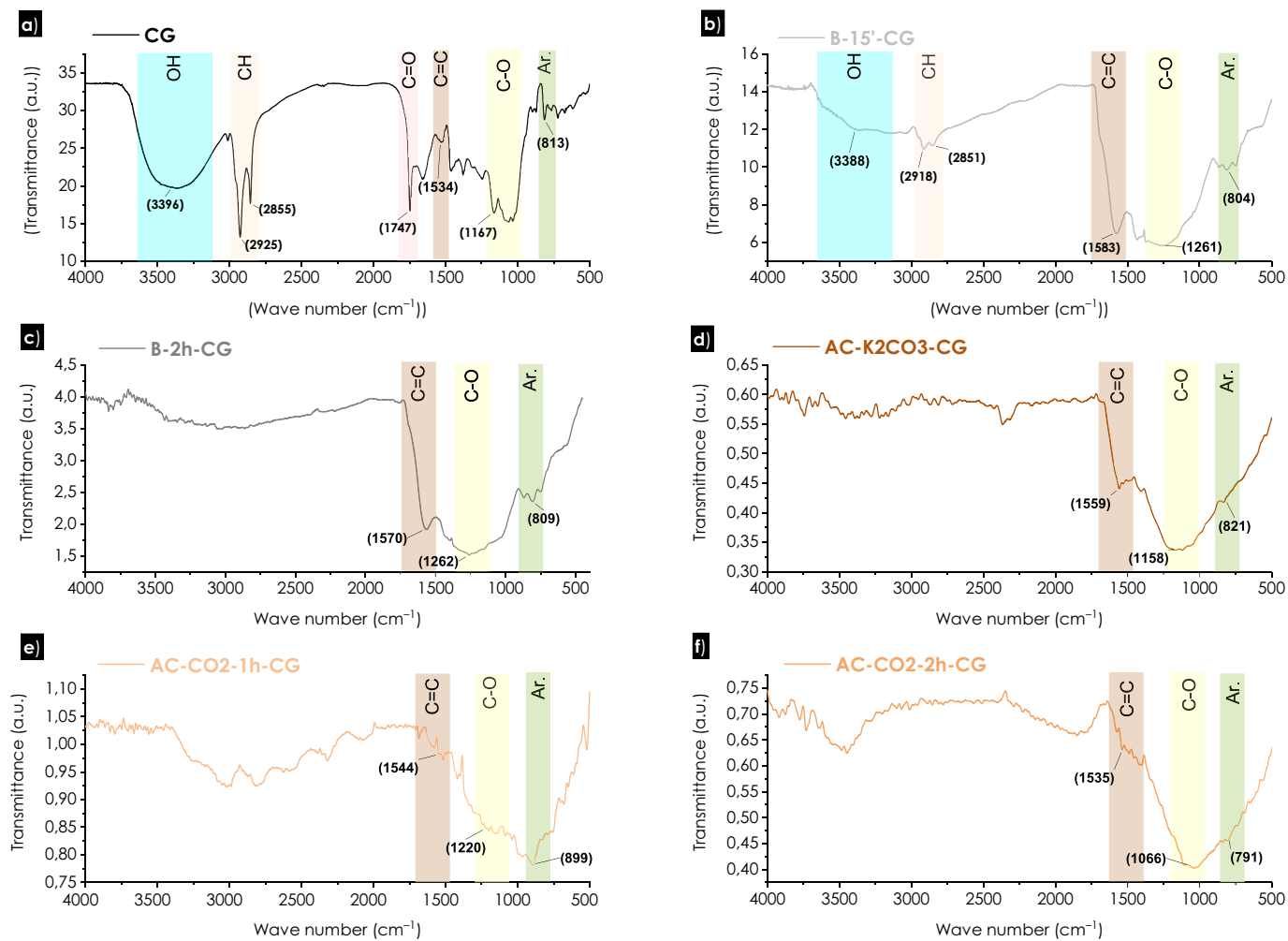


Fig. 10. FT-IR spectra of (a) coffee grounds, (b) B-(15')-CG, (c) B-(2 h)-CG, (d) AC-K₂CO₃-CG, (e) AC-CO₂(1 h)-CG and (f) AC-CO₂(2 h)-CG.

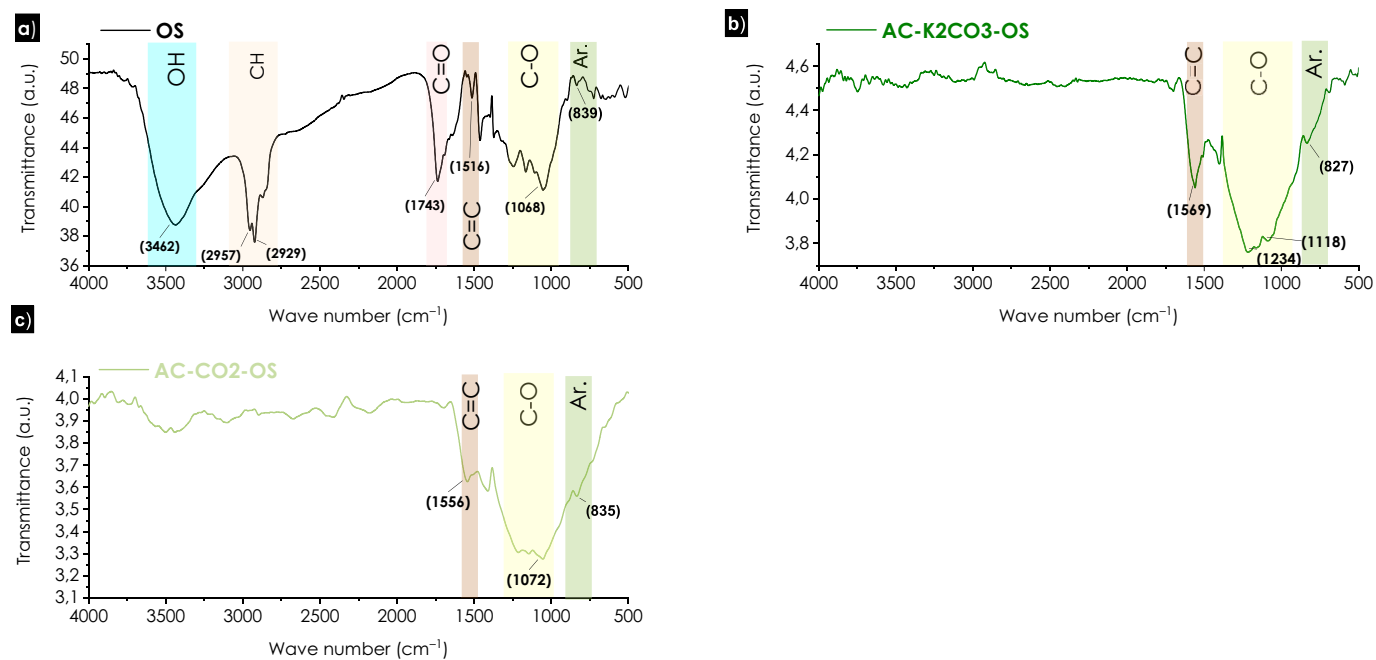


Fig. 11. FT-IR spectra of (a) olive stones, (b) AC-K₂CO₃-OS and (c) AC-CO₂-OS.

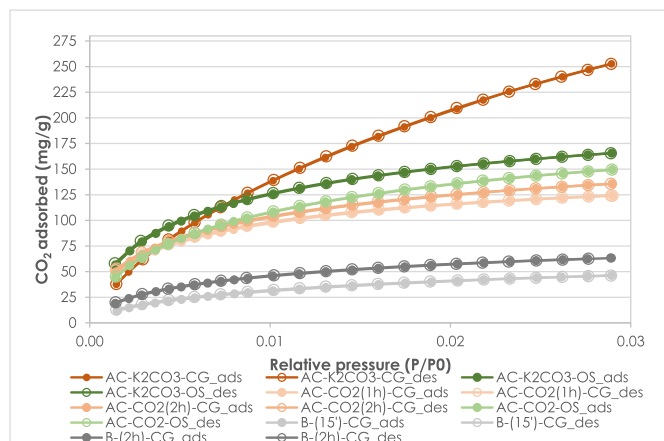


Fig. 12. CO₂ adsorption–desorption isotherms at 0 °C (DFT method) and a relative pressure range from 0.00 to 0.03.

The adsorption CO₂ test condition at atmospheric pressure was carried out to better evaluate its application in indoor. However, further tests under different relative pressure values are needed to have a full characterization and to explore all the possibilities on the field of CO₂ capture.

3.2.2. VOCs adsorption

Based on a chemical data sheet from the Occupational Safety and Health Administration (OSHA) (CARBON DIOXIDE, n.d.) (2-BUTANONE (METHYL ETHYL KETONE; MEK), n.d.; TOLUENE | Occupational Safety and Health Administration, 2020) and from the American Conference of Governmental Industrial Hygienists (ACGIH) (CARBON DIOXIDE, 2022; METHYL ETHYL KETONE, 2022; TOLUENE, ACGIH, 2022), acceptable levels in the workplace and the physical properties of the adsorbates used in this work are collected in Table 2. Threshold limit values (TLVs®) refer to airborne concentrations of chemical substances and are based solely on health factors; they are determined by a non-governmental scientific association (ACGIH). They represent conditions to which it is believed that nearly all workers may be repeatedly exposed, day after day, over a working lifetime, without experiencing adverse health effects, while the PELs (permissible exposure limits) constitute the regulatory limits on the concentration of a substance in the air set by OSHA. These limit values are given as a TWA (time-weighted average) and refer to the concentration for a conventional 8-h workday and a 40-h workweek to which it is believed that nearly all workers may be repeatedly exposed, day after day, for a working lifetime, without experiencing adverse effects.


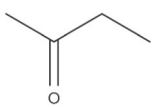
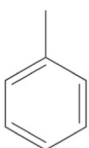
The initial toluene (14 ppm) and MEK (16 ppm) concentrations applied in the adsorption tests, corresponded to 7 % and 8 % of the PEL–TWA limits (200 ppm for MEK and toluene) set by OSHA and to 70 % and 21 % of the TLV–TWA limits (75 ppm for MEK and 20 ppm for toluene) set by ACGIH.

Adsorption of MEK and toluene on produced samples has been shown on Fig. 13 and Fig. 14 for the first cycle of exposure and for the second cycle, after the regeneration of the materials, to evaluate the reusability of the activated carbon. For sample AC-K₂CO₃-CG, the concentrations after 90 min of exposure for MEK were reduced to around 7 ppm, representing 59 % of the initial concentration. These results are comparable to those obtained from commercial AC-COM, and AC-CO₂-OS which removed 56 % and 55 % of MEK. AC-K₂CO₃-OS, AC-CO₂(2 h)-CG, AC-CO₂(1 h)-CG presented lower adsorption properties: 48 %, 40% and 36 % respectively. Both biochars (B-15'-CG and B-2 h-CG) showed a negligible adsorption capacity: 7 % and 5 %, respectively.

The chemically activated samples' (AC-K₂CO₃-CG, AC-K₂CO₃-OS) and AC-COM's ability to adsorb non-polar toluene is similar to that for polar MEK, suggesting that chemical activation promotes polar and non-

Table 2

Physical properties and acceptable concentration limits of the selected adsorbates.

Physical properties	Carbon dioxide	Methyl ethyl ketone	Toluene
Molecular structure			
Molecular weight	44 g/mol	72 g/mol	92 g/mol
Boiling point	−78.5 °C	79.6 °C	110.6 °C
Dipolar moment	0 D	2.76 D	0.31 D
Vapor pressure at 20 °C	716	71	21
Relative vapor density (air = 1)	1.53	2.42	3.14
Kinetic diameter ^a	0.330 nm	0.504 nm	0.568 nm
Limits			
OSHA PEL - TWA	5000 ppm	200 ppm	200 ppm
ACGIH TLV - TWA	5000 ppm	75 ppm	20 ppm

Abbreviations and Notes: OSHA = The Occupational Safety and Health Administration, PEL - TWA = Permissible Exposure Limits – Time Weighted Average, ACGIH = American Conference of Governmental Industrial Hygienists, TLV - TWA = Threshold Limit Values - Time Weighted Average

^a (La Rocca et al., 2019)

Table 3

Yield (wt%), proximate analysis (wt%), and pH_{pzc} of the precursors and carbon samples.

Sample	Yield (%)	Moisture (wt%)	Volatile matter (wt%)	Fixed carbon ^a (wt%)	Ashes (wt %)	pH _{pzc}
AC-K ₂ CO ₃ -CG	17	22.1	19.2	57.5	1.2	6.7
AC-K ₂ CO ₃ -OS	30	11.7	17.9	68.8	1.6	7.7
AC-CO ₂ -OS	21	10.3	15.5	73.3	0.9	9.3
AC-CO ₂ (2 h)-CG	20	10.5	23.2	60.6	5.7	10.4
AC-CO ₂ (1 h)-CG	20	9.9	22.4	62.1	5.6	9.4
B-(2 h)-CG	24	5.7	27.8	62.0	4.5	10.7
B-(15')-CG	28	5.4	34.5	56.0	4.1	10.5
CG	–	9.4	78.0	12.0	0.6	n.d.
OS	–	8.0	77.0	14.0	0.5	n.d.
AC-COM	–	6.9	11.0	76.0	6.1	Basic ^b

Abbreviations and notes: n.d. = not determined

^a Fixed carbon = 100 - (moisture + volatile matter + ashes).

^b Declared in the datasheet.

polar groups at carbons' surfaces. In the case of physically activated carbons, we noted a decrease in the adsorption: −15 % for AC-CO₂-OS, −11 % for AC-CO₂(2 h)-CG, and −16 % for AC-CO₂(1 h)-CG.

Other research study (Zhu et al., 2020) specified that physical adsorption was noted to occur in three stages: (a) the adsorption of VOC molecules at the external surface of the adsorbent via convection, axial dispersion, and particle diffusion. This rate is determined by the specific surface area. (b) The pollutant molecules can then diffuse through the porous structure of the activated carbon onto smaller pores. As reported elsewhere, the extent of the diffusion is dependent on the size of the molecules and the pore structure and volume of the activated carbon (Le-Minh et al., 2018). (c) In the final stage, the adsorbate is adsorbed onto the adsorbent and, when equilibrium occurs, the ratio of the micro-, meso-, and macropore volume is the dominant factor.

Adsorbent recyclability is another important indicator, as it determines the cost of the adsorption process and the possibility of

Table 4
Textural properties of the samples.

Sample	N ₂					CO ₂				
	^a SSA m ² /g	^b V _{total} cm ³ /g	^c V _{micro} cm ³ /g	% micro	^b V _{meso} cm ³ /g	% meso	^d SSA m ² /g	^d V _{total} cm ³ /g	^d V _{narrow} cm ³ /g	% narrow
AC-K ₂ CO ₃ -CG	1597	0.736	0.580	79	0.156	21	1487	0.527	0.24	46
AC-K ₂ CO ₃ -OS	274	0.121	0.097	80	0.024	20	870	0.221	0.17	77
AC-CO ₂ -OS	432	0.181	0.148	82	0.033	18	778	0.205	0.16	78
AC-CO ₂ (2 h)-CG	159	0.063	0.057	90	0.006	10	716	0.184	0.14	76
AC-CO ₂ (1 h)-CG	173	0.064	0.059	92	0.005	8	649	0.159	0.13	82
B-(2 h)-CG	n.d.	n.d.	n.d.	n.d.	n.d.	n.d.	331	0.088	0.07	80
B-(15')-CG	n.d.	n.d.	n.d.	n.d.	n.d.	n.d.	251	0.070	0.05	71
AC-COM	^e 1200									

SSA = specific surface area, V_{total} = total pore volume, V_{micro} = micropore volume; V_{meso} = mesopore volume; n.d. = not determined.

^a Determined via the BET eq. (P/P₀ < 0.1).

^b Single-point adsorption total pore volume of pores smaller than 40.6 nm at P/P₀ = 0.95.

^c Measured using the t-plot method.

^d Determined via the DFT method.

^e Declared in the datasheet.

Table 5
CO₂ and VOCs adsorption capacity.

Sample	CO ₂ (mg/g)	MEK (mg/g)		Toluene (mg/g)	
		I cycle	II cycle	I cycle	II cycle
AC-K ₂ CO ₃ -CG	253	3210	2765	2618	2547
AC-K ₂ CO ₃ -OS	166	2611	2304	2332	1999
AC-CO ₂ -OS	145	2992	2406	1904	1880
AC-CO ₂ (2 h)-CG	136	2176	1818	1380	1119
AC-CO ₂ (1 h)-CG	124	1958	1638	952	690
B-(2 h)-CG	63	381	0	428	24
B-(15')-CG	46	272	0	238	0
AC-COM	–	3046	2560	2618	2309

commercialization. Fig. 13 and Fig. 14 show that the results obtained from adsorption by regenerated samples (Cycle II) still represent a fairly good ability to VOCs capture, implying that the spent materials can be reused in an eco-friendly way without much loss (maximum of 8 %) in activity after the treatment. Similar results were obtained by Shah et al. (Shah et al., 2014), who found regeneration efficiencies >90 % at temperatures above 120 °C for MEK; however, this was after a longer regeneration period (two hours), which is associated with higher energy consumption.

As demonstrated in Fig. 13b and Fig. 14b the correlation coefficients are 0.94 and 0.87, indicating that the adsorption capacity of the VOCs increases with the increase of the specific surface area of the adsorbent. This is related to the fact that a larger specific surface area determines the presence of more pores on the carbon's surface, and VOCs can be captured more easily. Although micropores play a key role in the adsorption of VOCs at low concentrations (ppbv and ppmv) in indoor environments (Foster et al., 1992), mesopores in the AC-K₂CO₃-CG sample could also enhance the diffusion of the VOC molecules in the micropores (Anfruns et al., 2011), thus increasing the adsorption capacity.

The kinetic diameters of MEK and toluene are 0.504 nm and 0.568 nm, respectively. To better understand and illustrate which pores are able to capture both of these molecules, Table S2 presents the volume and percentage of pores larger than the kinetic diameter of MEK (>0.50 nm) and toluene (>0.57 nm) that were obtained using the previous DFT method. All the samples show a higher adsorption capacity for MEK, which is the adsorbate with the highest dipole moment. It has been also demonstrated that, for each type of produced carbon, there is a greater content of pores >0.50 nm than >0.57 nm, which means that there are more possible active sites for MEK molecules than for toluene. In fact, a decrease of 11–16 % in toluene removal and 36–51 % in the adsorption capacity was observed for AC-CO₂-OS, AC-CO₂(2 h)-CG, and AC-CO₂(1 h)-CG. This phenomenon was not observed for AC-K₂CO₃-CG, AC-

K₂CO₃-OS, or AC-COM, for which the percentages of adsorbed MEK and toluene after 90 min reached almost the same values; however, the adsorption capacity decreased by around 11–18 %.

The adsorption mechanisms of volatile organic compounds may be controlled by the following interactions: the hydrophobic effect, π - π bonds, hydrogen bonds, Van der Waals interactions, and covalent and electrostatic interactions (Zhang et al., 2017). Changes in adsorption can be explained by the presence of heteroatoms, which determine the apparent acidity or basicity of the activated carbon surface. As a result, molecules that interact with carbon in a specific way can adsorb more strongly and in greater amounts when the functional groups are present (Salame and Bandosz, 1999). The adsorption performance of aromatic molecules with benzene rings takes place via the electron donor-acceptor reaction, involving π electrons on the activated carbon surface, aromatic rings, and basic functional groups (π -electron-rich functional groups), as demonstrated in (Li et al., 2020; Konan et al., 2019). On the other hand, the electron-withdrawing carbonyl group found in the produced sample may reduce its surface electron density on the graphite-like activated carbon layer, thus weakening the π - π conjugated effect between toluene and the adsorbent (Zhao et al., 2018; Lei et al., 2020).

The much lower toluene adsorption recorded for the physically activated carbons may also be related to their lower aromaticity. The FT-IR results (Fig. 11 and Fig. 12) indicate that the intensity of the peaks associated with the aromatic C=C stretching for the AC-CO₂-OS, AC-CO₂(2 h)-CG, and AC-CO₂(1 h)-CG samples are lower than for AC-K₂CO₃-CG and AC-K₂CO₃-OS, indicating a larger number of aromatic groups, which may be responsible for the higher adsorption capacity.

Table 6 compares the type of precursor, processing parameters, type of activating agents, and surface area of various activated carbons with depollution properties. The results obtained for the adsorption of VOCs under static conditions were found to be comparably higher than the results of most other adsorbents in the literature. However, regarding VOC adsorption, there are only a few data obtained in conditions similar to those used in our study (low VOCs concentration, a static adsorption setup) which try to simulate as better as possible a real indoor environment. Most adsorption data are collected under high concentrations (100 to 1000 ppm), which does not simulate the realistic indoor operating conditions (VOCs concentrations in the range of the limits of TLV-TWA) at which gaseous indoor contaminant air cleaning devices/materials could be applied. In the study conducted by Takada and co-authors (Takada et al., 2022), activated carbon produced from buckwheat hulls with an SSA of 1300 m²/g was able to remove 36 % of toluene after 90 min of exposure. However, a higher initial concentration was applied (220 ppm), and the adsorption capacity also depends on the initial concentration. As indicated in the literature, when the

Table 6
Comparison of biomass-derived carbons for air pollutant adsorption.

Carbon precursor	Sample nomenclature	Activation conditions		Specific surface area [m ² /g]	Adsorbate	Ads. capacity	Experimental conditions	Ref
		Activation agent	Time and temperature					
Rice husk	KOH-AC	KOH (impregnation)	2 h 750 °C	1439	CO ₂	251 mg/g	P = 1 bar T = 0 °C	(Wang et al., 2022a)
<i>Arundo donax</i>	KLB2	KOH		1122	CO ₂	277 mg/g	P = 1 bar T = 0 °C	(Singh et al., 2017)
Coffee grounds	CG800-1	K ₂ CO ₃ (mixing)	1 h 800 °C	1692	CO ₂	102 mg/g and 316 mg/g	P = 0.15 bar and P = 1 bar, T = 0 °C	(Kim, 2020)
Tea waste	K-VT	KOH (impregnation)	2 h 600 °C	470	CO ₂	102 mg/g	TGA method at 25 °C	(Tahmasebpour et al., 2023)
The stems of <i>Diplotaxis acris</i>	AC	1. Pyrolysis 2. 85 % H ₃ PO ₄ (impregnation)	2 h 550 °C	40	Benzene	5.4 mg/g	Static adsorption test in 25 °C, initial conc. 313 ppm	(El-Hashemy and Alotaibi, 2023)
Buckwheat Hull	Unactivated adsorbent and K ₂ CO ₃ -activated adsorbent	None and K ₂ CO ₃ (impregnation)	2 h 800 °C	240 (biochar) 1300 (AC)	Toluene	18 % removed by biochar and 36 % by AC, during 90 min exposure	Static adsorption test in Tedlar® bag, Initial concentration 230 ppm T = 15–16 °C m _{AC} = 0.2 g	(Takada et al., 2022)
Commercial coal based	CAC	–		842	Toluene	65 mg/m ³	Dynamic adsorption (fixed bed reactor), Initial concentration 32 ppm, T = 39 °C, ambient pressure	(Li et al., 2021)
Sewage-sludge	SB-P-AGK-AW	KOH (mixing)	1 h 700 °C	990	Toluene, MEK Limonene	350 mg/g 220 mg/g 640 mg/g	Dynamic adsorption, initial concentration 100 ppm for toluene and 50 ppm for MEK and limonene	(Anfruns et al., 2011)
Black cumin		ZnCl ₂ (impregnation)	1 h 550 °C	1213	BTX: Benzene, toluene, xylene	495 mg/g 580 mg/g 674 mg/g	Dynamic adsorption, single and multi-component system, initial conc. 20 mg/l T = 25 °C,	(Batur and Kutluay, 2022)
Banana peel		KOH (impregnation)	3 h 800 °C	3746	Benzene, toluene	2149 mg/g 2195 mg/g	Pressure 12.7 kPa (for benzene) and 3.8 kPa (for toluene)	(Shen, 2020)
Corn cob	CAC450–800	KOH (impregnation)	3 h 800 °C	1618	H ₂ S, NH ₃	165 mg/g 191 mg/g	Static adsorption, H ₂ S 400 ppm NH ₃ 400 ppm	(Berhe Gebreegziabher et al., 2019)
Coffee grounds	AC-450	KOH (impregnation)	2 h 750 °C	1422	H ₂ S	139 mg/g	Static adsorption 400 ppm	(Wang et al., 2022b)
<i>Tilia cordata</i> residues	TCAC44	H ₃ PO ₄ (impregnation)	2 h 650 °C	110	Benzene	58 mg/g for 35 °C + 95 % RH to 121 mg/g for 25 °C + 15 % RH	Batch reactor, initial conc. 10 to 200 mg/m ³ , at different RH, for 70 mins	(Isinkaralar, 2023)
<i>Aesculus hippocastanum</i> L.	AC-KN	ZnCl ₂ (impregnation)	1 h 600 °C	1858	Formaldehyde, BTEX	638 to 1114 µg/g	2 l reactor, in batch analysis for formaldehyded in modified sorbent tube (Tenax TA) for BTEX	(Isinkaralar et al., 2023)
Walnut shell	WC-4	–	2 h 800 °C	555	Toluene	133 mg/g	Dynamic adsorption, initial conc. 200 ppm	(Gan et al., 2021)

contaminant concentration in the air phase is low, the diffusion rate decreases. The VOC molecules instantly adsorb onto the particle surface and they may not reach the deepest pores (Khazraei, 2014).

For instance, Shen (Shen, 2020) investigated the adsorption behaviors of ACs derived from banana peels on benzene and toluene at 25 °C. The adsorption capacities of the obtained carbons were 2149 mg/g and 2195 mg/g for benzene and toluene, respectively. However, a dynamic method of adsorption measurements was applied. Batur and Kutluay (Batur and Kutluay, 2022) produced AC from black cumin via chemical activation and explored its adsorption capacity for benzene, toluene, and xylene (BTX) vapors at low initial concentrations (20 mg/l for single or 20 mg/l + 10 mg/l for multi-component systems). They observed that activated carbon shows a lower adsorption capacity in the multi-

component system due to competitive adsorption, which depends on the properties of the VOCs (e.g., polarity, boiling point, molecular weight).

4. Conclusions

This work focuses on the use of biomass wastes such as coffee grounds and olive stones in physical and chemical activation, as a sustainable approach to obtaining activated carbon. After their development and the study of the main properties and characteristic, the following conclusions were drawn:

Methyl Ethyl Ketone

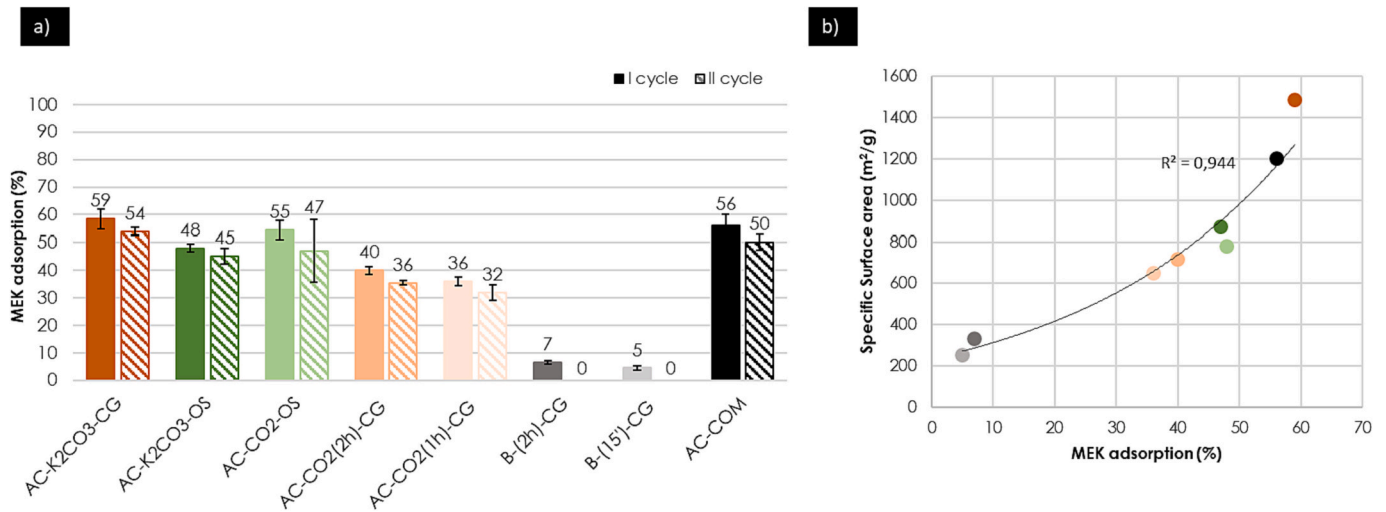


Fig. 13. (a) MEK adsorption (first and the second cycle) and (b) the relationship between specific surface area and adsorbed MEK.

Toluene

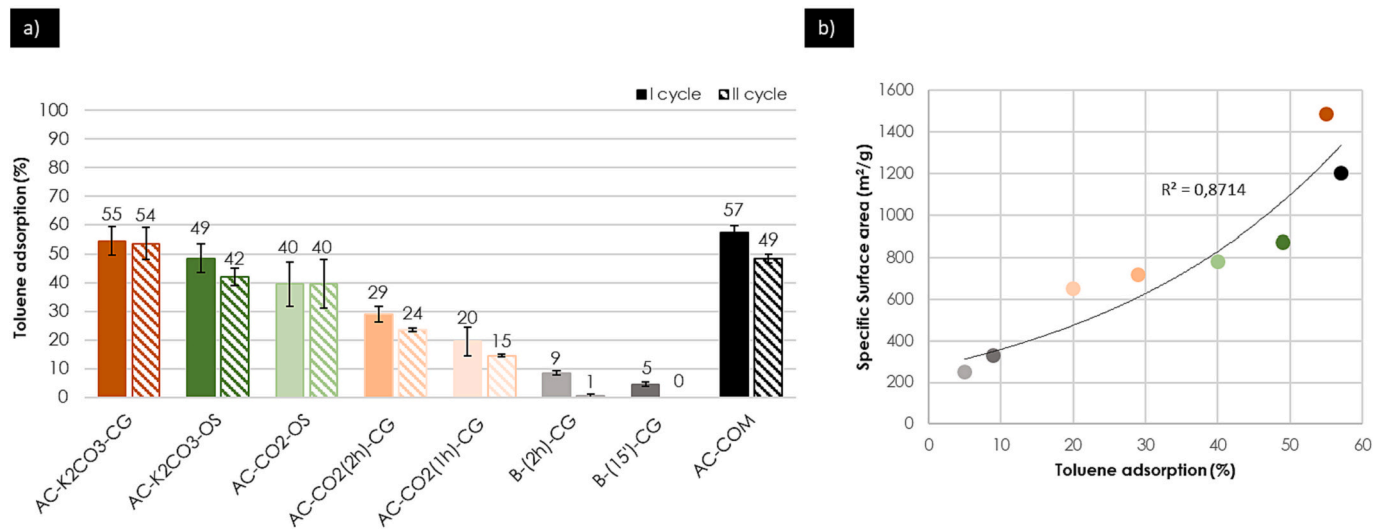


Fig. 14. (a) Toluene adsorption (first and the second cycle) and (b) relationship between the specific surface area and adsorbed toluene.

- The chemical activation of coffee grounds by K₂CO₃ (AC-K₂CO₃-CG) at 800 °C is the most effective process condition for establishing the highest degree of porosity and the development of a large surface area (1487 m²/g) and total pore volume (0.527 cm³) obtained from CO₂ isotherms.
- The pore size distribution of the activated carbons mainly resides in a very narrow region of ultra-micropores (0.5–0.6 nm).
- We demonstrated that, via the chemical activation of coffee grounds, it is possible to obtain materials with textural properties and a capacity for VOCs adsorption comparable to commercial activated carbon, measured under ambient conditions.
- The VOCs adsorption results indicated the high adsorption capacity for activated carbons (MEK 3210–1958 mg/g and toluene 2618–952 mg/g) and removal efficiency (MEK 59%–36% and toluene 55%–20%) of the prepared ACs for low MEK and toluene concentrations (14–16 ppm).
- The adsorption capacity of toluene was always lower for each sample, perhaps due to toluene’s higher kinetic diameter.

- Regeneration at 100 °C for 1 h promoted the effective removal of MEK and toluene.
- Chemically activated carbon produced from the coffee grounds showed promising results for CO₂ uptake (253 mg/g); however, further adsorption tests under indoor conditions are needed.

Overall, the AC-K₂CO₃-CG was selected as the best-performing sample, and it could potentially be used for the removal of VOCs and the improvement of indoor air quality, as its high specific surface area, total pore volume, and adsorption capacity could be beneficial for air purification via filters integrated into ventilation systems or other materials.

This study is expected to help future authors on this topic, by providing a simple and cost-effective strategy to:

- assess the valorization potential of specific organic wastes locally available in large quantities;
- develop non-conventional depolluting materials;

- optimize in a few steps the production process of non-conventional depolluting materials;
- compare new materials with commercial ones under indoor real condition, even at laboratory scale;
- close the loop while simultaneously providing a solution to others environmental problems;

CRediT authorship contribution statement

Natalia Czerwinska: Conceptualization, Data curation, Investigation, Methodology, Writing – original draft, Writing – review & editing. **Chiara Giosuè:** Conceptualization, Data curation, Investigation, Methodology, Writing – review & editing. **Ines Matos:** Investigation, Methodology. **Simona Sabbatini:** Investigation, Writing – review & editing. **Maria Letizia Ruello:** Conceptualization, Methodology, Supervision, Validation, Writing – review & editing. **Maria Bernardo:** Conceptualization, Funding acquisition, Methodology, Resources, Supervision, Writing – review & editing.

Declaration of competing interest

The authors declare that they have no known competing financial interests or personal relationships that could have appeared to influence the work reported in this paper.

Data availability

I have shared the data in the manuscript and in the supplementary materials

Acknowledgments

The production of carbons was carried out during a STSM (short-term scientific mission) at the Nova University of Lisbon in Portugal, under the supervision of Dr. Maria Bernardo and Dr. Ines Matos; it was supported by Greening Cost Action CA18224 (www.cost.eu). The co-grant for research contract was provided thanks to the program 'FSE-REACT-EU, PON Ricerca e Innovazione 2014-2020 DM 1062/2021'. This work was also funded by the Associate Laboratory for Green Chemistry, LAQV, which is financed by national funds from FCT/MCTES (UIDB/50006/2020 and UIDP/50006/2020). Maria Bernardo thanks FCT (Fundação para a Ciência e Tecnologia) for funding her through program DL 57/2016—Norma transitória.

We would also like to thank COMELT S.p.A for providing the activated carbon Carbosorb PCF.

Appendix A. Supplementary data

Supplementary data to this article can be found online at <https://doi.org/10.1016/j.scitotenv.2024.169898>.

References

- 2-BUTANONE (METHYL ETHYL KETONE; MEK) | Occupational Safety and Health Administration, (n.d.). <https://www.osha.gov/chemicaldata/680> (accessed July 7, 2023).
- Abdul Manap, N.R., Shamsudin, R., Maghpor, M.N., Abdul Hamid, M.A., Jalar, A., 2018. Adsorption isotherm and kinetic study of gas-solid system of formaldehyde on oil palm mesocarp bio-char: pyrolysis effect. *J. Environ. Chem. Eng.* 6 (1), 970–983. <https://doi.org/10.1016/j.jece.2017.12.067>.
- Adinata, D., Wan Daud, W.M.A., Aroua, M.K., 2007. Preparation and characterization of activated carbon from palm shell by chemical activation with K_2CO_3 . *Bioresour. Technol.* 98 (1), 145–149. <https://doi.org/10.1016/j.biortech.2005.11.006>.
- Allahkarami, E., Dehghan Monfared, A., Silva, L.F.O., Dotto, G.L., 2023. Toward a mechanistic understanding of adsorption behavior of phenol onto a novel activated carbon composite. *Sci. Rep.* 13 (1), 167. <https://doi.org/10.1038/s41598-023-27507-5>.
- Andamon, M.M., Rajagopalan, P., Woo, J., 2023. Evaluation of ventilation in Australian school classrooms using long-term indoor CO_2 concentration measurements. *Build. Environ.* 237, 110313 <https://doi.org/10.1016/j.buildenv.2023.110313>.
- Anfruns, A., Martin, M.J., Montes-Morán, M.A., 2011. Removal of odorous VOCs using sludge-based adsorbents. *Chem. Eng. J.* 166 (3), 1022–1031. <https://doi.org/10.1016/j.cej.2010.11.095>.
- Ballesteros, L.F., Teixeira, J.A., Mussatto, S.I., 2014. Chemical, functional, and structural properties of spent coffee grounds and coffee Silverskin. *Food Bioprocess Technol.* 7, 3493–3503. <https://doi.org/10.1007/s11947-014-1349-z>.
- Batur, E., Kutluay, S., 2022. Dynamic adsorption behavior of benzene, toluene, and xylene VOCs in single- and multi-component systems by activated carbon derived from defatted black cumin (*Nigella sativa* L.) biowaste. *J. Environ. Chem. Eng.* 10 (3), 107565 <https://doi.org/10.1016/j.jece.2022.107565>.
- Bedoui, A., Souissi-Najar, S., Idris, S.S., Rahman, N.A., Ouederni, A., 2021. Thermal behaviour of impregnated olive stones with phosphoric acid via TGA-MS. *C. R. Chim.* 24 (S1), 1–14. <https://doi.org/10.5802/crchim.118>.
- Benallou Benzekri, M., Benderdouche, N., Bestani, B., Douara, N., Duclaux, L., 2018. Valorization of olive stones into a granular activated carbon for the removal of methylene blue in batch and fixed bed modes. *J. Mater. Environ. Sci.* 9, 272–284. <https://doi.org/10.26872/jmes.2018.9.1.31>.
- Berhe Gebreegziabher, T., Wang, S., Nam, H., 2019. Adsorption of H_2S , NH_3 and TMA from indoor air using porous corn cob activated carbon: isotherm and kinetics study. *J. Environ. Chem. Eng.* 7 (4), 103234 <https://doi.org/10.1016/j.jece.2019.103234>.
- Bernardo, M., Rodrigues, S., Lapa, N., Matos, I., Lemos, F., Batista, M.K.S., Carvalho, A. P., Fonseca, I., 2016. High efficacy on diclofenac removal by activated carbon produced from potato peel waste. *Int. J. Environ. Sci. Technol.* 13, 1989–2000. <https://doi.org/10.1007/s13762-016-1030-3>.
- CARBON DIOXIDE | Occupational Safety and Health Administration, (n.d.). <https://www.osha.gov/chemicaldata/183> (accessed July 7, 2023).
- CARBON DIOXIDE, ACGIH, 2022. <https://www.acgih.org/carbon-dioxide/>. (Accessed 26 August 2023).
- Cuhadaroglu, D., Uygun, O.A., 2008. Production and characterization of activated carbon from a bituminous coal by chemical activation. *Afr. J. Biotechnol.* 7, 20. <https://doi.org/10.5897/AJB08.588>.
- Diao, Y., Walawender, W.P., Fan, L.T., 2002. Activated carbons prepared from phosphoric acid activation of grain sorghum. *Bioresour. Technol.* 81 (1), 45–52. [https://doi.org/10.1016/S0960-8524\(01\)00100-6](https://doi.org/10.1016/S0960-8524(01)00100-6).
- Dias, J.M., Alvim-Ferraz, M.C.M., Almeida, M.F., Rivera-Utrilla, J., Sánchez-Polo, M., 2007. Waste materials for activated carbon preparation and its use in aqueous-phase treatment: a review. *J. Environ. Manag.* 85 (4), 833–846. <https://doi.org/10.1016/j.jenvman.2007.07.031>.
- El-Hashemy, M.A.E.-S., Alotaibi, N.F., 2023. Purification of benzene-laden air by static adsorption of benzene onto activated carbon prepared from *Diplotaxis acris* biomass. *Biomass Convers. Biorefinery* 13, 1763–1777. <https://doi.org/10.1007/s13399-021-01462-5>.
- European Commission, 2023. Olive oil, Detailed information on the market situation, price developments, balance sheets, production and trade. <https://agriculture.ec.europa.eu/data-and-analysis/markets/price-data/price-monitoring-sector/olive-oil-en>. (Accessed 18 August 2023).
- Eurostat, 2022. Rise in EU population working from home. <https://ec.europa.eu/eurostat/web/products-eurostat-news/-/ddn-20221108-1>. (Accessed 3 August 2023).
- Foster, K.L., Fuerman, R.G., Economy, J., Larson, S.M., Rood, M.J., 1992. Adsorption characteristics of trace volatile organic compounds in gas streams onto activated carbon fibers. *Chem. Mater.* 4 (5), 1068–1073. <https://doi.org/10.1021/cm00023a026>.
- Galhetas, M., Mestre, A.S., Pinto, M.L., Gulyurtlu, I., Lopes, H., Carvalho, A.P., 2014. Chars from gasification of coal and pine activated with K_2CO_3 : acetaminophen and caffeine adsorption from aqueous solutions. *J. Colloid Interface Sci.* 433, 94–103. <https://doi.org/10.1016/j.jcis.2014.06.043>.
- Gan, F., Cheng, B., Jin, Z., Dai, Z., Wang, B., Yang, L., Jiang, X., 2021. Hierarchical porous biochar from plant-based biomass through selectively removing lignin carbon from biochar for enhanced removal of toluene. *Chemosphere* 279, 130514. <https://doi.org/10.1016/j.chemosphere.2021.130514>.
- García-Mateos, F.J., Rosas, J.M., Rodríguez-Mirasol, J., Cordero, T., 2016. Biomass waste carbon materials as adsorbents for CO_2 capture under post-combustion conditions. *Front. Mater.* 3, 23 <https://doi.org/10.3389/fmats.2016.00023>.
- Georgin, J., Franco, D.S.P., Schadeck Netto, M., Allasia, D., Foletto, E.L., Oliveira, L.F.S., Dotto, G.L., 2021. Transforming shrub waste into a high-efficiency adsorbent: application of *Physalis peruviana* chalice treated with strong acid to remove the 2,4-dichlorophenoxyacetic acid herbicide. *J. Environ. Chem. Eng.* 9 (1), 104574 <https://doi.org/10.1016/j.jece.2020.104574>.
- Giosuè, C., Pierpaoli, M., di Perna, C., Citterio, B., Mangiaterra, G., Ruello, M.L., Tittarelli, F., 2023. Properties of an innovative multi-functional finish for the improvement of indoor air quality. *Build. Environ.* 233, 110091 <https://doi.org/10.1016/j.buildenv.2023.110091>.
- Grassi, P., Netto, M.S., Jahn, S.L., Georgin, J., Franco, D.S.P., Sillanpää, M., Meili, L., Silva, L.F.O., 2022. Conversion of foliar residues of *Sansevieria trifasciata* into adsorbents: dye adsorption in continuous and discontinuous systems. *Environ. Sci. Pollut. Res.* 30 (4), 9688–9698. <https://doi.org/10.1007/s11356-022-22857-5>.
- Grøntoft, T., Marinacis, O., 2018. Indoor air pollution impact on cultural heritage in an urban and a rural location in Romania: the national military museum in Bucharest and the Tismana monastery in Gorj County. *Herit. Sci.* 6 (1), 73. <https://doi.org/10.1186/s40494-018-0238-6>.
- Grøntoft, T., López-Aparicio, S., Scharff, M., Ryhl-Svendsen, M., Andrade, G., Obarzanowski, M., Thickett, D., 2011. Impact loads of air pollutants on paintings: performance evaluation by modeling for microclimate frames. *J. Am. Inst. Conserv.* 50 (2), 105–122. <https://doi.org/10.1179/019713611804480953>.
- Gundogdu, A., Duran, C., Senturk, H.B., Soylak, M., Imamoglu, M., Onal, Y., 2013. Physicochemical characteristics of a novel activated carbon produced from tea

- industry waste. *J. Anal. Appl. Pyrolysis* 104, 249–259. <https://doi.org/10.1016/j.jaap.2013.07.008>.
- Hayashi, J., Horikawa, T., Takeda, I., Muroyama, K., Nasir Ani, F., 2002. Preparing activated carbon from various nutshells by chemical activation with K_2CO_3 . *Carbon* 40 (13), 2381–2386. [https://doi.org/10.1016/S0008-6223\(02\)00118-5](https://doi.org/10.1016/S0008-6223(02)00118-5).
- Hazzaa, R., Hussein, M., 2015. Adsorption of cationic dye from aqueous solution onto activated carbon prepared from olive stones. *Environ. Technol. Innov.* 4, 36–51. <https://doi.org/10.1016/j.eti.2015.04.002>.
- Hongqiang, L., Yongshui, Q., Xu, J., 2014. Microwave-Assisted Conversion of Lignin. In: *Biofuels and Biorefineries*, 3, pp. 61–82. https://doi.org/10.1007/978-94-017-9612-5_4.
- International Coffee Organization, 2022. What's new. <https://ico.org>. (Accessed 14 September 2022).
- Isinkaralar, K., 2023. Improving the adsorption performance of non-polar benzene vapor by using lignin-based activated carbon. *Environ. Sci. Pollut. Res.* 30 (50), 108706–108719. <https://doi.org/10.1007/s11356-023-30046-1>.
- Isinkaralar, K., Gullu, G., Turkyilmaz, A., 2023. Experimental study of formaldehyde and BTEX adsorption onto activated carbon from lignocellulosic biomass. *Biomass Convers. Biorefinery* 13 (5), 4279–4289. <https://doi.org/10.1007/s13399-021-02287-y>.
- Justo Alonso, M., Moazami, T.N., Liu, P., Jørgensen, R.B., Mathisen, H.M., 2022. Assessing the indoor air quality and their predictor variable in 21 home offices during the Covid-19 pandemic in Norway. *Build. Environ.* 225, 109580 <https://doi.org/10.1016/j.buildenv.2022.109580>.
- Kerkhoff, C.M., da Boit Martinello, K., Franco, D.S.P., Netto, M.S., Georgin, J., Foletto, E. L., Piccilli, D.G.A., Silva, L.F.O., Dotto, G.L., 2021. Adsorption of ketoprofen and paracetamol and treatment of a synthetic mixture by novel porous carbon derived from *Butia capitata* endocarp. *J. Mol. Liq.* 339, 117184 <https://doi.org/10.1016/j.molliq.2021.117184>.
- Khazraei, V.A., 2014. Predicting the Performance of Activated Carbon Filters at Low Concentrations Using Accelerated Test Data. PhD thesis. Concordiam University. <https://core.ac.uk/download/pdf/211517627.pdf>. (Accessed 20 August 2023).
- Kim, M.-J., 2020. Simple synthesis of spent coffee ground-based microporous carbons using K_2CO_3 as an activation agent and their application to CO_2 capture. *Chem. Eng. J.* 397, 125404 <https://doi.org/10.1016/j.cej.2020.125404>.
- Kim, S., Kim, H.-J., Moon, S.-J., 2006. Evaluation of VOC emissions from building finishing materials using a small chamber and VOC analyser. *Indoor Built Environ.* 15 (6), 511–523. <https://doi.org/10.1177/1420326X060672040>.
- Kishibayev, K.K., Serafin, J., Tokpayev, R.R., Khavaza, T.N., Atchabarova, A.A., Abduakhytova, D.A., Ibraimov, Z.T., Srenescek-Nazzal, J., 2021. Physical and chemical properties of activated carbon synthesized from plant wastes and shungite for CO_2 capture. *J. Environ. Chem. Eng.* 9 (6), 106798 <https://doi.org/10.1016/j.jece.2021.106798>.
- Klepeis, N.E., Nelson, W.C., Ott, W.R., Robinson, J.P., Tsang, A.M., Switzer, P., Behar, J. V., Hern, S.C., Engelmann, W.H., 2001. The National Human Activity Pattern Survey (NHAPS): a resource for assessing exposure to environmental pollutants. *J. Expo. Sci. Environ. Epidemiol.* 11 (3), 231–252. <https://doi.org/10.1038/sj.jea.7500165>.
- Konan, A.T.S., Richard, R., Andriantsiferana, C., Yao, K.B., Manero, M.H., 2019. Low-cost activated carbon for adsorption and heterogeneous ozonation of phenolic wastewater. *Desalin. Water* 163, 336–346. <https://doi.org/10.5004/dwt.2019.24804>.
- La Rocca, T., Carretier, E., Dhaler, D., Louradour, E., Truong, T., Moulin, P., 2019. Purification of pharmaceutical solvents by pervaporation through hybrid silica membranes. *Membranes* 9 (7), 76. <https://doi.org/10.3390/membranes9070076>.
- Laksaci, H., Khelifi, A., Belhamdi, B., Trari, M., 2017. Valorization of coffee grounds into activated carbon using physico-chemical activation by KOH/CO_2 . *J. Environ. Chem. Eng.* 5 (5), 5061–5066. <https://doi.org/10.1016/j.jece.2017.09.036>.
- Lapuerta, M., Hernández, J.J., Pazo, A., López, J., 2008. Gasification and co-gasification of biomass wastes: effect of the biomass origin and the gasifier operating conditions. *Fuel Process. Technol.* 89 (9), 828–837. <https://doi.org/10.1016/j.fuproc.2008.02.001>.
- Lazarotto, J.S., Da Boit Martinello, K., Georgin, J., Franco, D.S.P., Netto, M.S., Piccilli, D. G.A., Silva, L.F.O., Lima, E.C., Dotto, G.L., 2021. Preparation of activated carbon from the residues of the mushroom (*Agaricus bisporus*) production chain for the adsorption of the 2,4-dichlorophenoxyacetic herbicide. *J. Environ. Chem. Eng.* 9 (6), 106843 <https://doi.org/10.1016/j.jece.2021.106843>.
- Lei, B., Xie, H., Chen, S., Liu, B., Zhou, G., 2020. Control of pore structure and surface chemistry of activated carbon derived from waste *Zanthoxylum bungeanum* branches for toluene removal in air. *Environ. Sci. Pollut. Res.* 27, 27072–27092. <https://doi.org/10.1007/s11356-020-09115-2>.
- Le-Minh, N., Sivret, E.C., Shammay, A., Stuetz, R.M., 2018. Factors affecting the adsorption of gaseous environmental odors by activated carbon: a critical review. *Crit. Rev. Environ. Sci. Technol.* 48 (4), 341–375. <https://doi.org/10.1080/10643389.2018.1460984>.
- Li, J., Ma, X., Wu, H., Yang, L., 2021. Adsorption of low-concentration VOCs on modified activated carbons in a humid atmosphere. *Energy & Fuel* 35 (6), 5090–5100. <https://doi.org/10.1021/acs.energyfuels.0c03971>.
- Li, X., Luo, X., Dou, L., Chen, K., 2016. Preparation and characterization of K_2CO_3 -activated Kraft lignin carbon. *BioResources* 11 (1), 2096–2108. <https://doi.org/10.15376/biores.11.1.2096-2108>.
- Li, X., Zhang, L., Yang, Z., Wang, P., Yan, Y., Ran, J., 2020. Adsorption materials for volatile organic compounds (VOCs) and the key factors for VOCs adsorption process: a review. *Sep. Purif. Technol.* 235, 116213 <https://doi.org/10.1016/j.seppur.2019.116213>.
- Liu, C., Wang, H., Sun, J., Wang, Y., 2014. Catalytic fast pyrolysis of lignocellulosic biomass. *Chem. Soc. Rev.* 43 (22), 7594–7623. <https://doi.org/10.1039/c3cs60414d>.
- Liu, X., Zhu, H., Gong, L., Jiang, L., Lin, D., Yang, K., 2022. New insights into hierarchical pore size and level of concentration in efficient removal of toluene vapor by activated carbon. *Sci. Total Environ.* 853, 158719 <https://doi.org/10.1016/j.scitotenv.2022.158719>.
- Liu, X.-Y., Huang, M., Ma, H.-L., Zhang, Z., Gao, J.-M., Zhu, Y.-L., Han, X., Guo, X., 2010. Preparation of a carbon-based solid acid catalyst by sulfonating activated carbon in a chemical reduction process. *Mol. Basel Switz.* 15 (10), 7188–7196. <https://doi.org/10.3390/molecules15107188>.
- Lobato-Peralta, D.R., Ayala-Cortés, A., Longoria, A., Pacheco-Catalán, D.E., Okoye, P.U., Villafán-Vidales, H.L., Arancibia-Bulnes, C.A., Cuentas-Gallegos, A.K., 2022. Activated carbons obtained by environmentally friendly activation using solar energy for their use in neutral electrolyte supercapacitors. *J. Energy Storage* 52, 104888. <https://doi.org/10.1016/j.est.2022.104888>.
- Lykiema, J., Sing, K.S.W., Haber, J., Kerker, M., Wolfram, E., Block, J.H., Churaev, N.V., Everet, D.H., Hansen, R.S., Haul, R.A.W., Hightower, J.W., Hunter, R.J., 1984. Prepared for Publication by the Subcommittee on Reporting Gas Adsorption Data Consisting of K. S. W. SING (UK, Chairman); D. H. EVERETT (UK); R. A. W. HAUL (FRG); L. MOSCOU (Netherlands); R. A. PIEROTTI (USA); J. ROUQUEROL (France); T. SIEMIENIEWSKA (Poland), p. 17.
- Madureira, J., Alvim-Ferraz, M., Rodrigues, S., Gonçalves, C., Azevedo, M., Pinto, E., Mayan, O., 2009. Indoor air quality in schools and health symptoms among Portuguese teachers. *Hum. Ecol. Risk Assess.* 15 (1), 159–169. <https://doi.org/10.1080/10807030802615881>.
- Maqbool, Q., Czerwinska, N., Giosue, C., Sabbatini, S., Ruello, M.L., Tittarelli, F., 2022. New waste-derived TiO₂ nanoparticles as a potential photocatalytic additive for lime based indoor finishings. *J. Clean. Prod.* 373, 133853 <https://doi.org/10.1016/j.jclepro.2022.133853>.
- Mestre, A., Freire, C., Pires, J., Carvalho, A., Pinto, M., 2014. High performance microspherical activated carbons for methane storage and landfill gas or biogas upgrade. *J. Mater. Chem. A* 2 (37), 15337–15344. <https://doi.org/10.1039/C4TA0342J>.
- Mestre, A.S., Hesse, F., Freire, C., Ania, C.O., Carvalho, A.P., 2019. Chemically activated high grade nanoporous carbons from low density renewable biomass (Agave sisalana) for the removal of pharmaceuticals. *J. Colloid Interface Sci.* 536, 681–693. <https://doi.org/10.1016/j.jcis.2018.10.081>.
- METHYL ETHYL KETONE, ACGIH, 2022. <https://www.acgih.org/methyl-ethyl-ketone-2/>. (Accessed 26 August 2023).
- Missia, D.A., Demetriou, E., Michael, N., Tolis, E.I., Bartzis, J.G., 2010. Indoor exposure from building materials: a field study. *Atmos. Environ.* 44 (35), 4388–4395. <https://doi.org/10.1016/j.atmosenv.2010.07.049>.
- Mochizuki, Y., Bud, J., Byambajav, E., Tsubouchi, N., 2022. Influence of ammonia treatment on the CO_2 adsorption of activated carbon. *J. Environ. Chem. Eng.* 10 (2), 107273 <https://doi.org/10.1016/j.jece.2022.107273>.
- Mokhati, A., Benturki, O., Kecira, Z., Bernardo, M., Matos, I., Lapa, N., Ventura, M., Soares, O.S.G.P., Rego, A.M., Fonseca, I.M., 2021. Nanoporous carbons prepared from argan nutshells as potential removal agents of diclofenac and paroxetine. *J. Mol. Liq.* 326, 115368 <https://doi.org/10.1016/j.molliq.2021.115368>.
- Mukhtar, A., Mellon, N., Saqib, S., Lee, S., Bustam, M., 2020. Extension of BET theory to CO_2 adsorption isotherms for ultra-microporosity of covalent organic polymer. *SN Appl. Sci.* 2, 1–4. <https://doi.org/10.1007/s42452-020-2968-9>.
- Nascimento, V.X., Schnorr, C., Lütke, S.F., Da Silva, M.C.F., Machado Machado, F., Thue, P.S., Lima, É.C., Vieillard, J., Silva, L.F.O., Dotto, G.L., 2023. Adsorptive features of magnetic activated carbons prepared by a one-step process towards brilliant blue dye. *Molecules* 28 (4), 1821. <https://doi.org/10.3390/molecules28041821>.
- Nieto-Márquez, A., De Mateo, M., Barrios, A., García-Soto, M.D.M.D.L.F., Narros, A., 2023. Improving indoor air quality by using photocatalytic paints. *Real case study at the Technical University of Madrid, atmospheric. Pollut. Res.* 14 (8), 101827 <https://doi.org/10.1016/j.apr.2023.101827>.
- Noh, J.S., Schwarz, J.A., 1989. Estimation of the point of zero charge of simple oxides by mass titration. *J. Colloid Interface Sci.* 130 (1), 157–164. [https://doi.org/10.1016/0021-9797\(89\)90086-6](https://doi.org/10.1016/0021-9797(89)90086-6).
- Oliveira, M., Tutikian, B., Milanés Batista, C., Silva, L., 2020. Atmospheric contaminations and bad conservation effects in Roman mosaics and mortars of Itálica. *J. Clean. Prod.* 248, 119250 <https://doi.org/10.1016/j.jclepro.2019.119250>.
- Palmieri, S., Pierpaoli, M., Riderelli, L., Qi, S., Ruello, M.L., 2020. Preparation and characterization of an electrospun PLA-Cyclodextrins composite for simultaneous high-efficiency PM and VOC removal. *J. Compos. Sci.* 4 (2), 79. <https://doi.org/10.3390/jcs4020079>.
- Pandiarajan, A., Kamaraj, R., Vasudevan, S., Vasudevan, S., 2018. OPAC (orange peel activated carbon) derived from waste orange peel for the adsorption of chlorophenoxyacetic acid herbicides from water: adsorption isotherm, kinetic modelling and thermodynamic studies. *Bioresour. Technol.* 261, 329–341. <https://doi.org/10.1016/j.biortech.2018.04.005>.
- Park, M.H., Yun, Y.S., Cho, S.Y., Kim, N.R., Jin, H.-J., 2016. Waste coffee grounds-derived nanoporous carbon nanosheets for supercapacitors. *Carbon Lett.* 19 (1), 66–71. <https://doi.org/10.5714/CL.2016.19.066>.
- Pereira, H.A., da Boit Martinello, K., Vieira, Y., Diel, J.C., Netto, M.S., Reske, G.D., Lorenzetti, E., Silva, L.F.O., Burgo, T.A.L., Dotto, G.L., 2023. Adsorptive behavior of multi-walled carbon nanotubes immobilized magnetic nanoparticles for removing selected pesticides from aqueous matrices. *Chemosphere* 325, 138384. <https://doi.org/10.1016/j.chemosphere.2023.138384>.

- Pérez Marín, A.B., Aguilar, M.I., Meseguer, V.F., Ortuño, J.F., Sáez, J., Lloréns, M., 2009. Biosorption of chromium (III) by orange (*Citrus cinensis*) waste: batch and continuous studies. *Chem. Eng. J.* 155 (1-2), 199–206. <https://doi.org/10.1016/j.cej.2009.07.034>.
- Pérez-Lombard, L., Ortiz, J., Pout, C., 2008. A review on buildings energy consumption information. *Energy Buildings* 40 (3), 394–398. <https://doi.org/10.1016/j.enbuild.2007.03.007>.
- Pigatto, R.S., Franco, D.S.P., Netto, M.S., Carissimi, É., Oliveira, L.F.S., Jahn, S.L., Dotto, G.L., 2020. An eco-friendly and low-cost strategy for groundwater defluorination: adsorption of fluoride onto calcinated sludge. *J. Environ. Chem. Eng.* 8 (6), 104546. <https://doi.org/10.1016/j.jece.2020.104546>.
- Ramírez Hernández, O., Boit, K., Blanco Donado, E., Silva, L., 2020. Hazardous thoracic and ultrafine particles from road dust in a Caribbean industrial city. *Urban Clim.* 33, 1–11. <https://doi.org/10.1016/j.uclim.2020.100655>.
- Rovelli, S., Cattaneo, A., Fazio, A., Spinazzè, A., Borghi, F., Campagnolo, D., Dossi, C., Cavallo, D.M., 2019. VOCs measurements in residential buildings: quantification via thermal desorption and assessment of indoor concentrations in a case-study. *Atmosphere* 10 (2), 57. <https://doi.org/10.3390/atmos10020057>.
- Saad, M.J., Chia, C., Zakaria, S., Sajab, M.S., Misran, S., Rahman, M.H. Bin Abdul, Chin, S.X., 2019. Physical and chemical properties of the Rice straw activated carbon produced from carbonization and KOH activation processes. *Sains Malays.* 48 (2), 385–391. <https://doi.org/10.17576/jsm-2019-4802-16>.
- Salame, I.I., Bandosz, T.J., 1999. Study of water adsorption on activated carbons with different degrees of surface oxidation. *J. Colloid Interface Sci.* 210 (2), 367–374. <https://doi.org/10.1006/jcis.1998.5918>.
- Salomón, Y.L.D.O., Georgin, J., Franco, D.S.P., Netto, M.S., Picilli, D.G.A., Foletto, E.L., Oliveira, L.F.S., Dotto, G.L., 2021. High-performance removal of 2,4-dichlorophenoxyacetic acid herbicide in water using activated carbon derived from queen palm fruit endocarp (*Syagrus romanzoffiana*). *J. Environ. Chem. Eng.* 9 (1), 104911. <https://doi.org/10.1016/j.jece.2020.104911>.
- Sanginés, P., Domínguez, M.P., Sánchez, F., San Miguel, G., 2015. Slow pyrolysis of olive stones in a rotary kiln: chemical and energy characterization of solid, gas, and condensable products. *J. Renew. Sustain. Energy* 7 (4), 043103. <https://doi.org/10.1063/1.4923442>.
- Schibuola, L., Tambani, C., 2021. High energy efficiency ventilation to limit COVID-19 contagion in school environments. *Energy Buildings* 240, 110882. <https://doi.org/10.1016/j.enbuild.2021.110882>.
- Sellaoui, L., Silva, L.F.O., Badawi, M., Ali, J., Favarin, N., Dotto, G.L., Erto, A., Chen, Z., 2021. Adsorption of ketoprofen and 2-nitrophenol on activated carbon prepared from winery wastes: a combined experimental and theoretical study. *J. Mol. Liq.* 333, 115906. <https://doi.org/10.1016/j.molliq.2021.115906>.
- Serafin, J., Dziejarski, B., Sreńscek-Nazzal, J., 2023. An innovative and environmentally friendly bioorganic synthesis of activated carbon based on olive stones and its potential application for CO₂ capture. *Sustain. Mater. Technol.* 38, e00717. <https://doi.org/10.1016/j.susmat.2023.e00717>.
- Sevilla, M., Díez, N., Fuentes, A.B., 2021. More sustainable chemical activation strategies for the production of porous carbons. *ChemSusChem* 14, 94–117. <https://doi.org/10.1002/cssc.202001838>.
- Shah, I.K., Pre, P., Alappat, B.J., 2014. Effect of thermal regeneration of spent activated carbon on volatile organic compound adsorption performances. *J. Taiwan Inst. Chem. Eng.* 45 (4), 1733–1738. <https://doi.org/10.1016/j.jtice.2014.01.006>.
- Shen, X., 2020. Record-high capture of volatile benzene and toluene enabled by activator implant-optimized banana peel-derived engineering carbonaceous adsorbents. *Environ. Int.* 143, 105774. <https://doi.org/10.1016/j.envint.2020.105774>.
- Silva, L.F.O., Pinto, D., Neckel, A., Oliveira, M.L.S., Sampaio, C.H., 2020a. Atmospheric nanocompounds on Lanzarote Island: vehicular exhaust and igneous geologic formation interactions. *Chemosphere* 254, 126822. <https://doi.org/10.1016/j.chemosphere.2020.126822>.
- Silva, L.F.O., Pinto, D., Neckel, A., Dotto, G.L., Oliveira, M.L.S., 2020b. The impact of air pollution on the rate of degradation of the fortress of Florianópolis Island, Brazil. *Chemosphere* 251, 126838. <https://doi.org/10.1016/j.chemosphere.2020.126838>.
- Silva, L.F.O., Pinto, D., Neckel, A., Oliveira, M.L.S., 2020c. An analysis of vehicular exhaust derived nanoparticles and historical Belgium fortress building interfaces. *Geosci. Front.* 11, 2053–2060. <https://doi.org/10.1016/j.gsf.2020.07.003>.
- Singh, G., Kim, I.Y., Lakhi, K.S., Srivastava, P., Naidu, R., Vinu, A., 2017. Single step synthesis of activated bio-carbons with a high surface area and their excellent CO₂ adsorption capacity. *Carbon* 116, 448–455. <https://doi.org/10.1016/j.carbon.2017.02.015>.
- Singh, G., Maria Ruban, A., Geng, X., Vinu, A., 2023. Recognizing the potential of K-salts, apart from KOH, for generating porous carbons using chemical activation. *Chem. Eng. J.* 451, 139045. <https://doi.org/10.1016/j.cej.2022.139045>.
- Singh, S., Parveen, N., Gupta, H., 2018. Adsorptive decontamination of rhodamine-B from water using banana peel powder: a biosorbent. *Environ. Technol. Innov.* 12, 189–195. <https://doi.org/10.1016/j.eti.2018.09.001>.
- Steinemann, A., 2015. Volatile emissions from common consumer products. *Air Qual. Atmos. Health* 8, 273–281. <https://doi.org/10.1007/s11869-015-0327-6>.
- Streit, A.F.M., Collazzo, G.C., Druzian, S.P., Verdi, R.S., Foletto, E.L., Oliveira, L.F.S., Dotto, G.L., 2021. Adsorption of ibuprofen, ketoprofen, and paracetamol onto activated carbon prepared from effluent treatment plant sludge of the beverage industry. *Chemosphere* 262, 128322. <https://doi.org/10.1016/j.chemosphere.2020.128322>.
- Tahmasebpoor, M., Iranvandi, M., Heidari, M., Azimi, B., Pevida, C., 2023. Development of novel waste tea-derived activated carbon promoted with SiO₂ nanoparticles as highly robust and easily fluidizable sorbent for low-temperature CO₂ capture. *J. Environ. Chem. Eng.* 11 (5), 110437. <https://doi.org/10.1016/j.jece.2023.110437>.
- Takada, T., Tanaka, R., Ono, R., 2022. Removal of volatile toluene using K₂CO₃-activated carbon adsorbents prepared from buckwheat Hull. *Pollutants* 2 (1), 12–20. <https://doi.org/10.3390/pollutants2010002>.
- Talakesh, M.M., Sadeghi, M., Chenar, M.P., Khosravi, A., 2012. Gas separation properties of poly(ethylene glycol)/poly(tetramethylene glycol) based polyurethane membranes. *J. Membr. Sci.* 415–416, 469–477. <https://doi.org/10.1016/j.memsci.2012.05.033>.
- Thommes, M., Kaneko, K., Neimark, A.V., Olivier, J.P., Rodriguez-Reinoso, F., Rouquerol, J., Sing, K.S.W., 2015. Physisorption of gases, with special reference to the evaluation of surface area and pore size distribution (IUPAC technical report). *Pure Appl. Chem.* 87 (9-10), 1051–1069. <https://doi.org/10.1515/pac-2014-1117>.
- TOLUENE | Occupational Safety and Health Administration, 2020. <https://www.osha.gov/chemicaldata/89>. (Accessed 7 July 2023).
- TOLUENE, ACGIH, 2022. <https://www.acgih.org/toluene/>. (Accessed 26 August 2023).
- Valvez, S., Maceiras, A., Santos, P., Reis, P.N.B., 2021. Olive stones as filler for polymer-based composites: a review. *Materials* 14 (4), 845. <https://doi.org/10.3390/ma14040845>.
- Vardon, D.R., Moser, B.R., Zheng, W., Witkin, K., Evangelista, R.L., Strathmann, T.J., Rajagopalan, K., Sharma, B.K., 2013. Complete utilization of spent coffee grounds to produce biodiesel, bio-oil, and biochar. *ACS Sustain. Chem. Eng.* 1 (10), 1286–1294. <https://doi.org/10.1021/sc400145w>.
- Wang, S., Lee, Y.-R., Won, Y., Kim, H., Jeong, S.-E., Wook Hwang, B., Ra Cho, A., Kim, J.-Y., Cheol Park, Y., Nam, H., Lee, D.-H., Kim, H., Jo, S.-H., 2022a. Development of high-performance adsorbent using KOH-impregnated rice husk-based activated carbon for indoor CO₂ adsorption. *Chem. Eng. J.* 437, 135378. <https://doi.org/10.1016/j.cej.2022.135378>.
- Wang, S., Nam, H., Lee, D., Nam, H., 2022b. H₂S gas adsorption study using copper impregnated on KOH activated carbon from coffee residue for indoor air purification. *J. Environ. Chem. Eng.* 10 (6), 108797. <https://doi.org/10.1016/j.jece.2022.108797>.
- Wei, X., Wu, S., Liu, P., Huang, S., Li, X., Yang, J., Wu, Y., 2023. Characterization of physicochemical properties of activated carbons prepared from penicillin mycelial residues and its adsorption properties for VOCs. *J. Environ. Chem. Eng.* 11 (3), 109733. <https://doi.org/10.1016/j.jece.2023.109733>.
- Wen, X., Liu, H., Zhang, L., Zhang, J., Fu, C., Shi, X., Chen, X., Mijowska, E., Chen, M.-J., Wang, D.-Y., 2019. Large-scale converting waste coffee grounds into functional carbon materials as high-efficient adsorbent for organic dyes. *Bioresour. Technol.* 272, 92–98. <https://doi.org/10.1016/j.biortech.2018.10.011>.
- Zhang, X., Gao, B., Creamer, A.E., Cao, C., Li, Y., 2017. Adsorption of VOCs onto engineered carbon materials: a review. *J. Hazard. Mater.* 338, 102–123. <https://doi.org/10.1016/j.jhazmat.2017.05.013>.
- Zhang, X., Xiang, W., Miao, X., Li, F., Qi, G., Cao, C., Ma, X., Chen, S., Zimmerman, A.R., Gao, B., 2022. Microwave biochars produced with activated carbon catalyst: characterization and sorption of volatile organic compounds (VOCs). *Sci. Total Environ.* 827, 153996. <https://doi.org/10.1016/j.scitotenv.2022.153996>.
- Zhao, X., Zeng, X., Qin, Y., Li, X., Zhu, T., Tang, X., 2018. An experimental and theoretical study of the adsorption removal of toluene and chlorobenzene on coconut shell derived carbon. *Chemosphere* 206, 285–292. <https://doi.org/10.1016/j.chemosphere.2018.04.126>.
- Zhu, L., Zhao, N., Tong, L., Lv, Y., 2018. Structural and adsorption characteristics of potassium carbonate activated biochar. *RSC Adv.* 8 (37), 21012–21019. <https://doi.org/10.1039/C8RA03335H>.
- Zhu, L., Shen, D., Luo, K.H., 2020. A critical review on VOCs adsorption by different porous materials: species, mechanisms and modification methods. *J. Hazard. Mater.* 389, 122102. <https://doi.org/10.1016/j.jhazmat.2020.122102>.
- Žuškin, E., Schachter, E.N., Mustajbegović, J., Pucarín-Cvetković, J., Doko-Jelinić, J., Mucić-Pucić, B., 2009. Indoor air pollution and effects on human health. *Period. Biol.* 111 (1), 37–40. <https://hrcak.srce.hr/35956>.